NEURONAL PHYSIOLOGICAL CORRELATION TO HEMODYNAMIC RESTING-STATE FLUCTUATIONS IN HEALTH AND DISEASES

by

Sowmya Aggarwal

BTech, Guru Gobind Singh Indraprastha University, India, 2009

MS in Biomedical Engineering, Carnegie Mellon University, 2013

Submitted to the Graduate Faculty of

Swanson School of Engineering in partial fulfillment

of the requirements for the degree of

Master of Science in Bioengineering

University of Pittsburgh

2016

UNIVERSITY OF PITTSBURGH

SWANSON SCHOOL OF ENGINEERING

This thesis was presented

by

Sowmya Aggarwal

It was defended on

April 26, 2016

and approved by

Kim Kang, Ph.D., Associate Professor, Departments of Radiology and Bioengineering

George Stetten, Ph.D., Professor, Department of Bioengineering

Thesis Advisor:

Alberto Luis Vazquez, Ph.D., Associate Professor, Departments of Radiology and Bioengineering

NEURONAL AND PHYSIOLOGICAL CORRELATION TO HEMODYNAMIC RESTING-STATE FLUCTUATIONS IN HEALTH AND DISEASES

Sowmya Aggarwal, M.S.

University of Pittsburgh, 2016

Low-frequency, spatially coherent fluctuations present in functional magnetic resonance imaging (fMRI) time series have had a tremendous impact on brain connectomics. To interpret the neurophysiological nature of changes in connectivity measured by hemodynamic signals, studies that investigate the dynamic relationship between neuronal and hemodynamic fluctuations are needed. Previously, our group used a transgenic animal model to simultaneously acquire bi-hemispheric images sensitive to neuronal and hemodynamic signals. We showed that hemodynamic connectivity is highly correlated with neuronal-connectivity in scans >5 min. This work used the same animal model and imaging method to calculate and compare the agreement between sliding window (SW) and dynamic conditional correlation (DCC) metrics. Transgenic GCaMP3 mice were used to simultaneously image ongoing changes in neuronal-activity (GCAMP) as well as hemodynamic measurements of blood oxygenation (OIS-BOLD, analogous to fMRI) from the same animals (n=6). Bi-hemispheric GCAMP and OIS-BOLD images were acquired at 10Hz from the exposed superior surface of the mouse brain under light ketamine anesthesia (30mg/kg/hr) for 5 to 20min periods. Pre-processing consisted of temporal band-pass filtering (0.02-0.20Hz). Then, k-means clustering was used on the GCAMP data to obtain 6 regions-of-interest. For each GCAMP and OIS-BOLD ROI time-series, we first examined the SW lengths for which the GCAMP and OIS-BOLD connectivity matrices were significantly

correlated ($r>0.47$ corresponds to $p<0.05$). Over non-overlapping windows, the average SW correlation and fraction of significant windows are reported. We then examined the temporal sampling resolution for which comparisons between the GCAMP DCC and OIS-BOLD DCC connectivity matrices were significantly correlated. GCAMP (neuronal) and OIS-BOLD (hemodynamic) time-series were used to calculate SW and DCC connectivity matrices. For each non-overlapping SW window, the inter-node connectivity of the GCAMP data was compared to that of the OIS-BOLD data and tested for significance using a correlation analysis. The average correlation shows significant relationships for window lengths over 20 sec, while the average fraction of significantly correlated windows was >80% for windows >40 sec. A similar analysis of the GCAMP and OIS-BOLD DCC connectivity shows that average significant relationships were observed for temporal resolution >1.4sec, and >80% of the comparisons were significant for temporal resolution >2.2sec.

TABLE OF CONTENTS

LIST OF TABLES

LIST OF FIGURES

PREFACE

All the work presented in this dissertation was conducted in Neuroimaging Laboratory, in the McGowan Institute at University of Pittsburgh, under the guidance of Dr. Alberto Luis Vazquez, associate professor in the departments of Radiology and Bioengineering. All procedures performed followed an experimental protocol approved by the University of Pittsburgh Institutional Animal Care. In this work, whenever a theory, figure or rationale for experiment are borrowed from other sources to explain previously existing technology, appropriate citations are provided. A version of abstract and results presented in this thesis was submitted to the Organization of Human Brain Mapping (OHBM) and it has been reviewed and selected by the OHBM review committee for traditional poster presentation and an oral session presentation at the OHBM Annual Meeting being held on June 30, 2016 in Geneva, Switzerland. Dr. Vazquez and I would like to thank Dr. Martin Lindquist, professor, Department of Biostatistics, John Hopkins University to have provided us with his MATLAB code for dynamic conditional correlation (DCC). We have analyzed our data with his DCC code and have used some introductory material in the manuscript with his approval and appropriate citations. We would also like to thank our colleague and co-author on the poster-abstract, Dr. Matthew Murphy for reviewing the original work and improving conceptualization along the process.

As the concluding part of my journey as a graduate student at the University of Pittsburgh, I would like to thank my family and my friends for their wonderful understanding and immense moral support throughout the adventure of my obtaining second Masters in Science degree in a row from two prestigious universities in Pittsburgh, Carnegie Mellon University and the University of Pittsburgh. Without their unconditional belief in me, the accomplishment of my academic goals would not have been nearly as possible.

Bioengineering, in the field of radiology, is a complex amalgamation of specialized domains in various sciences, such as genetics and functional neuroanatomy in biology, surgery and medicine, and electrical engineering, imaging-physics and analysis, machine learning, statistics and mathematics in the analytics and engineering domains. Merely possessing textbook knowledge is not enough to put a complex bioengineering idea to practice. I was fortunate to have been guided by my academic advisor, Dr. Alberto Luis Vazquez, who actively helped me in shaping my data analytics and several other scientific approaches in analyzing dynamic connectivity observed via neuroimaging of transgenic mice. This project is an extension of his previous work performed in his lab. Besides being the lead on this project, he was the supervisory author on this manuscript as well. I would also like to thank the thesis reviewers and dissertation committee members, Dr. Kim Kang and Dr. George Stetten, professors at the University of Pittsburgh and Carnegie Mellon to have reviewed my work presented below. They have been my teachers and mentors in several courses and research endeavors at the University of Pittsburgh, and, over the last two years, have helped me improve my scientific conceptualization and writing process as a researcher and a scientist.

For possessing all the grit, enabling students to achieve academic goals with their large amount of departmental work including scholarship approvals in the background, and offering

time and time again moral support to students, I would like to thank our Bioengineering Department Head, Dr. Sanjeev Govinddas Shroff, graduate coordinator, Nicholas Mance, and professor, graduate student coordinator and director of McGowan Institute of Regenerative Medicine, Dr. William J. Federspiel at the University of Pittsburgh.

In the end, I would like to say that none of this would have been remotely possible without everyone actively guiding and helping me along the way. While there are several people whom I would personally like to thank here for their compassion and invaluable inspiration, I wholeheartedly thank everyone for being a part of my unforgettable and enlightening journey as a student at the University of Pittsburgh.

1.0 INTRODUCTION

In the past two decades, functional magnetic resonance (fMRI) has proven to be a powerful technology for mapping brain functions; particularly to study the brain as a network of interacting regions. Functional connectivity represents an approach in which fMRI data is ideally used to investigate the neural activity of regions that are functionally connected even when they are anatomically distant. Practically, functional connectivity can be described as the synchrony in fMRI signal among regions that may or may not be neuronal in origin. This is because fMRI brain studies are sensitive to study small changes in the blood oxygen level-dependent (BOLD) signal which are induced by underlying neural activity. Changes in blood oxygenation are generally produced by the energetic demands of neurons to function. Areas of the brain which exhibit BOLD signal fluctuations correlated in time are then assumed to represent correlated neuronal activity and therefore considered to be functionally connected. Several research efforts aim at understanding hemodynamic and neuronal relationships, how brain multiple regions interact with one another and how this leads to functional neural-connections to be identified.

These BOLD signal fluctuations occur at low frequencies (≤0.1 Hz) and have been observed throughout the brain, and will be described in the next section. Functional connectivity can be studied during the performance of active tasks, such as finger tapping or visual

stimulation, as well as during rest, a condition in which a subject is not performing any active task and is simply instructed to remain still, with eyes closed or open while fixating a cross. In fact, it is well known that under resting conditions the brain is engaged in spontaneous activity which is not attributable to specific inputs or to the generation of specific output, but is intrinsically originated. The brain under normal physiological conditions is never idle, but always remains neuro-electrically and metabolically active.

1.1 RESTING STATE

Low-frequency changes in blood oxygenation (<0.1 Hz) measured using fMRI while the brain is in resting state (i.e., not performing any task), show specific bilateral patterns that outline known connectivity within brain networks. Previous studies of monkeys' visual cortex show a definitive relationship between hemodynamic fluctuations and the low frequency neural activity patterns [7]. Other studies that draw correspondences between the resting state neural activity and the low frequency fluctuations, found similarities while comparing the electrocorticography and magnetoencephalography with fMRI time-series measurements [7].

Techniques, such as EEG and fMRI are very different in that, EEG is limited to the surface of the brain while fMRI can cover the entire brain but the temporal resolution of EEG is considerably higher and comparable to the timescale of neural events, whereas that of fMRI is limited to several seconds by the hemodynamic response lag. As a consequence, fMRI can only characterize coherent activity in very low-frequency bands, i.e., ≤0.1 Hz, which are not directly

associated with the EEG activity in this frequency range. However, it appears that a correspondence does exist at a more abstract level, where— these low-frequency BOLD signal fluctuations track spontaneous changes in the envelope of these main EEG rhythms. Indeed, this correspondence is expected, since the BOLD and EEG signals share a common neurophysiological correlate, the local field potentials. Thus, there are other methods, besides fMRI, that are used to measure the fluctuations in the blood oxygenation levels more directly. These include mice studies where methods such as local cell potential measurement, optical imaging and direct electrode reading have been employed to detect and quantify neuronal changes for comparison with hemodynamic changes. (Mohajerani et. el. 2010[2], White et. el. 2011[6]).

1.2 INTRODUCTION TO TIME SERIES DATA ANALYSIS

A time series is a collection of observations of specific data-points obtained through continuous or discrete measurements taken over time. In bioengineering literature, time series is termed as signals. Time-series data is analyzed and widely studied because it provides useful information about the biological system that generate these signals. For our analysis, we observed cortical surface of the brain over a period of 5 minutes each at 10 Hz sampling rate. The recorded brain-images thus represent a collection of 2D image-data acquired over this time period. The product of the rows and columns of the 2D image is the total number of variables, each generating 1D time series signal, is our computational challenge that we want to analyze and study. Thus the data represents a multivariate time-series where each variable, mapping the

maximally resolvable region on the brain surface, represents a univariate time-series or a 1D signal. One of the main goals of time-series analysis is to identify the nature of phenomenon (in our case to study the resting state processes) represented by the sequence of observations. There are four major components of time-series – 1) trend, which is the rate of change in a time-series, 2) seasonal component, which is a periodic fluctuation, 3) cyclic component that is an unsystematic fluctuation and 4) irregular component, which represent the random/noisy residuals. An observed data represents stochastic process which can be described using a fitting mathematical model. In the time-domain analysis where the signal is a function of time, we can describe stationarity as a concept, wherein a signal is assumed to be statistically constant over time, i.e., for all the time points, the mean and the variance are the same. In other terms, the joint probability of distribution is invariant over time. Stationarity can be easily identified by eye-balling the data where all data-points appear to have similar values over time. Another concept is random time-series where the data-points oscillate about the same mean over time, such that their overall mean and variance are constant. A random model given by, $y_t = \mu + e_t$, is where μ is the mean of the time-series y_t, that's constant over time points, t. Due to oscillation around this constant mean (μ), e_t, is the independent error (residual) that not only has a zero mean but a constant variance. For resting state data, we make the following assumption, $\mu = 0$ and $y_t = e_t$. For our previous studies, we assumed that the noise, e_t, was represented by the random model such that it had constant mean and variance over time and thus represented a type of stationary process. For analyzing this stationary process, we used Pearson correlation coefficient to compare two time-series. However, for our current analysis, we realized (this section is explained in detail in chapter 2.0) that the e_t is a non-stationary component of the resting-state

time series and requires more complex statistical methods to describe correlation between any two resting-state (non-stationary) time series[8].

To understand functional connectivity in the regions of interest, it is often beneficial to demarcate the regions we want to study over a period of time. It is between these demarcated regions, called as regions of interest (ROIs), that we study the relationship or the connectivity to form powerful generalizations over a given period of time. For this study our main interest is not to make this generalization but to see how closely the two modalities of imaging, neural and hemodynamic, are correlated.

Let's say we have two time series data, of 5 minutes each observed from the same animal at 10 Hz sampling rate, such that one time-series represents neuronal data while the other hemodynamic, then each time series is composed of a collection of 2D images acquired over time. Once we identify the regions of interest (ROIs) within any 2D image, we can map those onto all images of the two time series, such that, we obtain time-series of ROIs themselves for the two modalities of interest. We then correlate the average intensities of all ROIs (n=6) in pairs (r=2) with each other in all combinations using Pearson correlation coefficient metric such that we now have C(n,r) (= n! / (r! (n - r)! = 15) distinct measures for each image over a time series. Each combination (calculated by Pearson correlation coefficient) of ROI-pair within a modality (say, neuronal data) is computed to then calculate similarity between the corresponding mutual combinations (Pearson correlation coefficient) of ROI-pairs within the other modality (hemodynamic data). Thus, we obtain C(n,r) measures of correlation per image for both the time series and to study the similarity between the two time-series (i.e., between the two modalities), we use additional methods as summarized below.

Now, since we are interested in studying the similarity between the two modalities given by two separate non-stationary time series having C(n,r) data points each, we can study how correlated the corresponding data points over time-series using methods (as described below) that enable us to analyze two non-stationary time-series. As mentioned earlier, for our previous analysis of the two modalities (Vazquez et. el. 2014 [7]), the metric of interest to study the demarcated ROIs, was Pearson correlation coefficient, however, as we will describe in chapter 2.0, why this method fails to capture the dynamic/non-stationary aspect of time-series, it will be clearer we are using different methods for our current analysis. In short, the Pearson correlation method that was designed to analyze data with constant mean and variance over time, did not represent an accurate method to tap the true nature of dynamic/non-stationary time-series that had variable variance over time. We have described in detail the state-of-the-art metrics that are more suitable to analyze and describe the relationship between the non-stationary time-series of C(n,r) data points of the two modalities of interest. For our analysis, the sliding window (SW) and dynamic conditional correlation (DCC), are the two main metrics of interest that we use for studying relationship between the two modalities given by non-stationary time-series. In summary, in order to adjudge the relationship between two ROIs within a modality, we use Pearson correlation coefficient, however, for the time-series analysis, i.e., the "between modality" analysis we use DCC and SW metrics that capture the non-stationarity in the data. Before discussing these methods to analyze the non-stationary time-series, let's discuss the methods we used for obtaining ROIs.

There are several techniques to automatically identify regions of interest. For our analysis, we will primarily focus on an iterative method, called as k-mean clustering (conceptually first described by J.B. MacQueen in 1967[10] as a general mathematical and

statistical process), to identify clusters of similar activity on the cortical surface of the brain. We measure this special similarity between say, neuronal activity, of different data-points (represented by all the cortical pixels in a 2D image in our case) using Pearson correlation coefficient. K-means clustering is then an unsupervised clustering algorithm that iteratively groups together data-points, pixels of image in our case, based on weighted distance metric (in our case, given by the similarity metric), into k number of clusters. Except for specifying the number of clusters/ROIs to be separated, k-means is fully automated in the sense that, the initial guesses for the centroid of these clusters can be randomly selected anywhere on the image. The method is powerful enough to iteratively converge and find appropriate centroids within an image, thus giving us regions of interest. For our analysis, we chose 6 clusters. Potential drawbacks with application of k-means clustering is, it may fail to converge and thus leave empty clusters behind. Another problem is, even if it converges in the end but we provided large number of clusters as the initial specifier, the algorithm will forcibly assign data points to spatially different clusters even if they are similar in activity to data-points in adjacent clusters. In our case, we found after experimentation that we were primarily interested in a totally of 6 clusters that not only converged effectively but provided us neuro-anatomically acceptable ROIs to work with.

Another powerful technique to study the time series data (that we did not prefer for this analysis) is independent component analysis (ICA) that uses a mathematical algorithm to decompose a set of signals into independent components also known as source signals. In particular, on the basis of the measured signals, ICA can reveal the hidden sources which have generated them, under the assumptions that sources are statistically independent. When applied

to fMRI, ICA is able to extract from the BOLD time series a number of independent components which are spatial maps associated with the time courses of the signal sources [2]. Each component can be interpreted as a network of similar BOLD activity. This may correspond to an actual functional network or in some cases to common physiological activity or neuroimaging artefacts. The studies using ICA have shown a high level of consistency in the reported components suggesting that ICA is a powerful technique that can be applied to the study of multiple connectivity patterns [1, 3]. However, a possible disadvantage of this technique is that the components are not always easy to interpret. ROI-based analysis and ICA represent two very different approaches of data analysis: the former is a hypothesis-driven method, which relies on the a priori definition of ROIs and which generates results that are limited to the given ROIs. In contrast, ICA is an exploratory, hypothesis-free method, which is designed to examine the general patterns of functional connectivity across brain regions and which generates results not at inter-regional level such the ROI-based analysis, but at network level. Even though

ROI-based analysis and ICA are very different in terms of methodology, the studies comparing the two techniques have provided similar results [8] where the functional networks that the two methods generate are quite overlapping [5–7]. This is expected, as they represent the same underlying connectivity, reflecting the synchrony of neural activity over spatially distinct regions. However, one needs to bear in mind the potential differences between the two techniques related to the effect of physiological activity, systemic changes and potential scanner drifts which can induce diffusely coherent signal fluctuations. **Previous studies at Neuroimaging Lab, in the McGowan Institute led by Dr. Alberto Luis Vazquez (Vazquez et. el.)[7]** have contributed to understanding the complex nature of the hemodynamic response

by exploring the neurophysiological contributions of low frequency fluctuations across mouse cortex and decreased brain connectivity using AD mouse-model. Statistical correlation method was used to measure the degree with which hemodynamic connectivity is associated with neuronal connectivity, and also related to vascular and metabolic signals.

2.0 DYNAMIC CORRELATION MODELING

Many equations and figures in chapter 2.0 of this document are taken from Lindquist et. el. 2014[8]. Interpreting the dynamic temporal fluctuations in FC can be difficult due to variation in BOLD signal mean and variance over time (Hutchison et al., 2013, [11]). This observed variation in BOLD signal mean and variance over time, makes the recorded neural/hemodynamic (GCaMP/OIS) signals non-stationary. Changes in both the strength and directionality of functional connections have been observed to vary across experimental runs [11]. As described earlier, a random model hat is given by, $y_t = \mu + e_t$, has the mean, μ, of the time-series constant which is equal to 0 in resting state as described in literature including [8] and [11]. Additionally, we mentioned that in resting state, the independent error (residual) e_t, neither has a zero mean or a constant variance, thus the signal that is now $y_t = e_t$, is non-stationary [11]. Thus, for our current analysis, we have made the following assumption of our resting state data, $\mu = 0$ and $y_t = e_t$. It is worth mentioning here that for our previous studies [Vazquez. et. el. [7]], we assumed that the noise, e_t, was represented by the random model such that it had constant mean and variance over time and thus represented a type of stationary process. For analyzing this stationary process, we used Pearson correlation coefficient to compare two time-series. However, for our current analysis, since we realized that the e_t is a non-stationary component of the resting-state time series, we are using more complex statistical

methods to describe correlation between any two resting-state (non-stationary) time series as described in [Lindquist et. el. [8]]. In other words, since the simple/traditional statistical correlation methods (Pearson correlation) for comparing the ROIs (6 neuronal clusters) and the modalities (GCaMP (neuronal) and OIS (hemodynamic), described in detail in chapter 3.0) with each other are insufficient, it is rational to explore methods that have proven to be successful in interpreting the dynamic changes in the measured cortical signals. Thus, to explore the degree with which hemodynamic connectivity was associated with neuronal, metabolic, and vascular connectivity measures, these volatility metrics that work effectively on non-stationary signals were generated to investigate correspondence (degree of correlation) between neural and hemodynamic connectivity based on blood-oxygenation- and CBV-sensitive OIS data.

Before discussing the concepts of conditional covariance and correlation, it is beneficial to discuss the concepts of simple covariance and correlation. Additionally, to understand the concept of how time plays an important role in conditional correlation concept, the concept of autocorrelation and jointly Gaussian random variables is discussed. [24]

The covariance of two random variables, X and Y is given as:

$$COV(X, Y) = E[(X - E[X])(Y - E[Y])] = E[XY] - E[X]E[Y]$$

where, E[X] is the expected value of the random variable X while, E[Y] is the expected value of the random variable Y. If the random variables are independent then the value of COV(X,Y) = 0. The correlation coefficient of X and Y is defined by:

$$\rho = \frac{COV(X,Y)}{\sigma_X \sigma_Y} = \frac{E[XY] - E[X][Y]}{\sigma_X \sigma_Y}$$

where the standard deviation of X is given by square root of variance of X,

$$\sigma_X = \sqrt{VAR(X)}$$

and the standard deviation of Y is given by square root of variance of Y,

$$\sigma_Y = \sqrt{VAR(Y)}$$

X and Y are said to be uncorrelated when $\rho_{xy} = 0$. It can be noted here that if the two random variables are independent then since their COV(X,Y) = 0, thus their correlation is zero as well. This concept will be useful when the conditional covariance between two time-series (two variables) will be discussed. Additionally, since we have multiple ROI's combinations as opposed to just a pair, we should discuss the concept of covariance matrix also.

To understand the concept of conditional covariance and correlation, it is important to discuss the concept of jointly Gaussian random variables. The jointly Gaussian random variables are frequently used to model signals in signal processing applications where noise is present. If the pdf of the jointly Gaussian random variable X is m, then, for the random variables, X_1, X_2, X_3, …, X_n are said to be jointly Gaussian if their joint pdf is given by [24]:

$$f_{\boldsymbol{x}}(\boldsymbol{x}) \triangleq f_{x_1,x_2..x_n(x_1,x_2,...x_n)} = \frac{exp\left\{-0.5(\boldsymbol{x}-\boldsymbol{m})^T K^{-1}(\boldsymbol{x}-\boldsymbol{m})\right\}}{2\pi^{n/2}|K|^{1/2}}$$

where **x** and **m** are column vectors defined by:

$$\boldsymbol{x} = \begin{bmatrix} x_1 \\ x_2 \\ \vdots \\ x_n \end{bmatrix}, \boldsymbol{m} = \begin{bmatrix} m_1 \\ m_2 \\ \vdots \\ m_n \end{bmatrix} = \begin{bmatrix} E[X_1] \\ E[X_2] \\ \vdots \\ E[X_n] \end{bmatrix}$$

And *K* is the covariance matrix that is defined by:

$$K = \begin{bmatrix} VAR(X_1) & COV(X_1, X_2) & \cdots & COV(X_1, X_n) \\ COV(X_2, X_1) & VAR(X_2) & \cdots & COV(X_2, X_n) \\ \vdots & \ddots & & \vdots \\ COV(X_n, X_1) & \cdots & & VAR(X_n) \end{bmatrix}$$

such that the covariance matrix for the 2D case is given by:

$$K = \begin{bmatrix} \sigma_1^2 & -\rho_{X,Y}\sigma_1\sigma_2 \\ -\rho_{X,Y}\sigma_1\sigma_2 & \sigma_2^2 \end{bmatrix}$$

Since the 'conditional' word in the time-series analytics-metric, condition correlation, 'also' refers to the concept of previous times (t-1,…,t-n), to understand how the concept of conditional covariance and correlation emerged, we must understand where the covariance and correlation is computed in a time-variant fashion. We will find that while revising the concept of autocorrelation, we use the concept of time to compute correlation. The same time-dependent concept of covariance and correlation can be applied to any two random variables as the simple correlation and covariance above to obtain "conditional" equations to compute the conditional covariance and correlation. In autocorrelation, the most important feature of time series is that successive values are not independent rather they are correlated with one another, i.e. they are serially correlated or autocorrelated [23]. Autocovariance and autocorrelation functions are important tools for describing the serial (or temporal) dependence structure of a univariate time series. Autocorrelation is a measure of the dependence of time series values at a certain time on the values at another time. It is the Pearson correlation between all the pairs of points in the time series with a given separation in time or lag. Positively autocorrelated series are sometimes

referred to as persistent because high values tend to follow high values and low values tend to follow low values. Negatively autocorrelated series are characterized by reversals from high to low values from one time segment to the next, and vice versa. Autocorrelation functions of deterministic data (like sine wave) persist over all time displacements, whereas autocorrelation functions of stochastic processes tend to zero for large time displacement (for zero-mean time series). The first order correlation (i.e. lag = 1) is the correlation coefficient of the first N − 1 observations [xt : t = 1, 2,...,N − 1] and the next N − 1 observations [xt : t = 2, 3,...,N]. It is given by the following formula:

$$r_k = \frac{\sum_{t=1}^{N-1}(x_t - \bar{x}_{(1)})(x_{t+1} - \bar{x}_2)}{\sqrt{\sum_{t=1}^{N-1}(x_t - \bar{x}_{(1)})^2}\sqrt{\sum_{t=1}^{N-1}(x_{t+1} - \bar{x}_{(2)})^2}}$$

where, $\overline{\chi_{(1)}}$ is the mean of the first *N-1* observations and so on.

Time series in the world of finance, where we assess risk of assets, the financial data acquired over time exhibit time-varying conditional standard deviations (volatility) and correlations. Here volatility is seen as a measure of the risk of assets, while correlations between time series play an important role in asset allocation and risk management (Tsay, 2006[12]). The problem of studying time-varying variances and correlations between multivariate time series, while relatively recent in the neuroimaging literature, has been extensively studied in the finance literature during the past few decades (for example, Bauwens et al., 2006 [13]). While numerous metrics for evaluating FC exist in current literature, for our current study we focused on sliding window (SW) (Handwerker et al., 2012 [14]) and dynamic conditional correlation (DCC) methods to handle volatility in the cortical data. Thus we have worked on the pair-wise

conditional-correlations between time courses from 6 regions of the brain to create a 6 x 6 correlation matrix for cortical data-analysis to model dynamic variances and correlations.

Briefly, sliding window (SW) is a method where a fixed length w is selected, and the data within that window is used to compute the correlation coefficient. The window is then moved step-wise across time, providing a time-varying measure of the correlation between brain regions. It is a very simple method to evaluate cortical signals. However, there are a number of drawbacks, such as selecting the window length is experimentation based. One size may not fit other types of similar datasets. Additionally, sliding window averages a lot of information over the window length, thus it may over generalize a signal. This very fact also makes it unsuitable to deal with fluctuations we are interested in capturing. Though it is conditional in nature and it considers w-1 (data at all time-points) to compute value for the current time point, it puts equal weight to all the previous observations that lie less than w time points in the past, but no weight to older observations (Engle, 2002 [15]).

Even though, SW is a good model to provide conditional correlation measures between cortical time-series, however, a parsimonious model called as generalized autoregressive conditional heteroscedastic (GARCH) model (Bollerslev, 1986 [16]) has been shown to efficiently model both dynamic variances and correlations. For any bivariate time-series, where we have time series from two ROIs (clusters), a univariate GARCH model (GARCH(1,1)) can output a very accurate correlation measure. The residual values are very close to the ground truth (an example of this plot is Fig. 1, where the line closest to the red line is the best model for dynamic correlation estimation). There is no parameter adjustment done here unlike SW. To analyze >2 ROIs, in order to generate a correlation matrix, an efficient way is to use multivariate GARCH model. In 2002, Engle [15] introduced a variant of the multivariate GARCH model,

called as the dynamic conditional correlation (DCC) model. DCC uses a sequential estimation scheme and a parsimonious parameterization that allows it to estimate very large covariance structures. This gives us a scalable opportunity to have multiple ROIs in our data for effective estimation of dynamic correlation between more than two brain regions. Besides being a step-up from SW, as for DCC all the parameters are effectively estimated through quasi-maximum likelihood methods and require no ad hoc parameter settings, DCC has been shown to be much better than multivariate GARCH models at effectively estimating both time varying variances and correlations as shown by Lebo and Box-Steffensmeier in their 2008 studies [17].

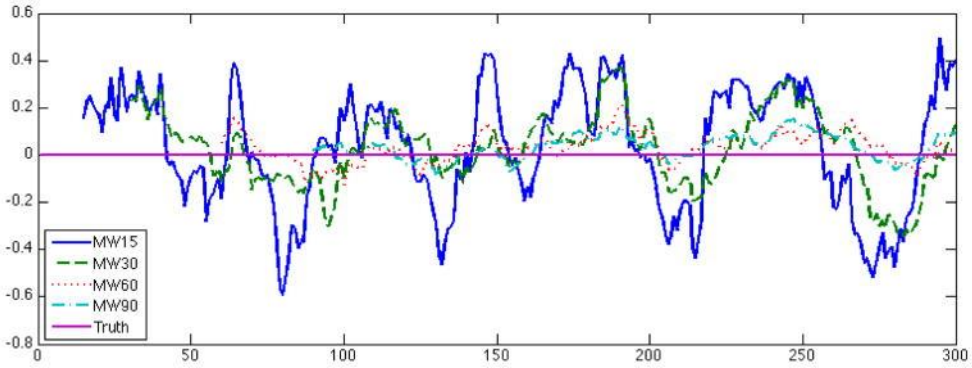

Figure 1. Parametric Conditional Correlation (SW) Simulation to Select Parameter. (This simulation result is imported from Lindquist et. el. 2014 [8])

In 2014, Martin Lindquist showed [8] for the first time that the lessons learnt from finance about DCC could be applied on neuroimaging data effectively in order to determine dynamic correlation. In his studies, his group investigated the properties of SW, DCC and other commonly used techniques in a series of simulation studies. His results indicated DCC showed

great promise in the analysis of dynamic FC. In addition to simulation, their group applied the DCC algorithm on fMRI time-series data and showed better performance in accurate estimation of dynamic correlation as compared with static/unconditional-correlation method used by previous groups on the same dataset.

2.1 UNDERSTANDING VOLATILITY MODELING METHODS: MARTIN LINDQUIST'S SIMULATION METHODS (LINDQUIST 2014) [8]

In order to show the effectiveness of a volatility modeling method, we can take two uncorrelation time series such that their means and variance over the time are different. Since they are uncorrelated, thus a robust dynamic correlation estimation method will be able to estimate the values closer to zero than farther away from it. This can be adjudged by observing the graphs of the residuals plotted around the ground truth. Let us assume that we are interested in studying the relationship between two time series $y_{1,t}$ and $y_{2,t}$, measured over two separate regions of interest (ROIs) in the brain, at equally spaced time points t=0,…, T.

Let $\mathbf{y_t} = (y_{1,t}, y_{2,t})^T$ be a vector containing the values of both time series at time t and assume that

$$\mathbf{y_t} = \boldsymbol{\mu_t} + \mathbf{e_t} \qquad (1)$$

where, $\mathbf{y_t} = (y_{1,t}, y_{2,t})^T$ is the conditional mean of yt using all information in the time series observed up to time t, denoted $E_{t-1}(\mathbf{y_t})$. The noise term $\mathbf{e_t}$ has mean zero and its conditional covariance matrix at time *t* can be expressed as

$$\sum_t = \begin{pmatrix} \sigma^2{}_{1,t} & \sigma^2{}_{12,t} \\ \sigma^2{}_{12,t} & \sigma^2{}_{2,t} \end{pmatrix} \quad (2)$$

Here the diagonal terms represent the conditional variance of $y_{i,t}$ using all information in the time course observed up to time t, written $\sigma^2_{\mathbf{i,t}} = E_{t-1}((\mathbf{y_{i,t}} - \boldsymbol{\mu}_{\mathbf{i,t}})^2)$ for i = 1, 2. The square root of this entity, σ_{it}, is typically referred to as the volatility of the time series. The off-diagonal term is $\sigma_{12,t} = \sigma_{1,t}\sigma_{2,t}\rho_t$ where eq. (3):

$$\rho_t = \frac{E_{t-1}((\mathbf{y_{1,t}} - \mu_{1,t})(\mathbf{y_{2,t}} - \mu_{2,t}))}{\sqrt{E_{t-1}\left((\mathbf{y_{1,t}} - \mu_{1,t})^2\right) E_{t-1}((\mathbf{y_{2,t}} - \mu_{2,t})^2)}} \quad (3)$$

represents the conditional correlation coefficient. The numerator here represents covariance between the two time series and the each term in the denominator is the standard deviation of the time series. A conditional correlation at time t is based on information observed up to time t − 1.

For resting state data, the following assumptions are made: $\mu_t = \mathbf{0}$ and $\mathbf{y}_t = \mathbf{e}_t$. Under this assumption, Eq. 3 simplifies as follows:

$$\rho_t = \frac{E_{t-1}((\mathbf{y_{1,t}})(\mathbf{y_{2,t}}))}{\sqrt{E_{t-1}\left((\mathbf{y_{1,t}})^2\right) E_{t-1}((\mathbf{y_{2,t}})^2)}} \quad (4)$$

The conditional covariance matrix defined in Eq. 2 can alternatively be written in matrix form as

$$\Sigma_t = D_t R_t D_t \tag{5}$$

where D_t is a diagonal matrix consisting of the conditional standard deviations of the time series, i.e.$D_t = diag\{\sigma_{1,t}, \sigma_{2,t}\}$ and R_t is the correlation matrix,

$$R_t = \begin{pmatrix} 1 & \rho_t \\ \rho_t & 1 \end{pmatrix} \tag{6}$$

The terms D_t and R_t define as the components of the $\sum_t$ .Thus, a vector containing both time series, y_t (that's made up of two univariate time-series) that has a mean zero and has only the error component that we model, can be represented as follows from equations (1), (2), (3) and (6) above:

$$y_t = (y_{1,t}, y_{2,t})^T = \mathbf{e}_t = \Sigma_t = D_t R_t D_t = \begin{bmatrix} \sigma_{1,t} & 0 \\ 0 & \sigma_{2,t} \end{bmatrix} \begin{bmatrix} 1 & \rho_t \\ \rho_t & 1 \end{bmatrix} \begin{bmatrix} \sigma_{1,t} & 0 \\ 0 & \sigma_{2,t} \end{bmatrix} \tag{7}$$

Thus in developing methods for estimating the components of the conditional covariance matrix, only the following unknown quantities, $\sigma^2_{1,t}$, $\sigma^2_{2,t}$ and ρ_t are estimated. Following volatility models to estimate the elements of the covariance matrix are discussed briefly:

2.2 SLIDING-WINDOW TECHNIQUE

Sliding-window correlations have been metrics of interest in the recent neuroimaging literature (Allen et al., 2012[18]). Here, a time window of fixed length w is selected, and data points within that window are used to calculate the correlation coefficients. The window is then moved across time and a new correlation coefficient is computed for each time point.

The window specifically defined using only past values provides a more suitable estimate of the conditional correlation defined in Eq. 4. Equal weight to all observations that lie less than w time points in the past and zero weight to all older observations are allotted. For the case when $\mu = 0$, the sliding-window conditional variance at time t as follows:

$$\hat{\sigma}_{i,t}^2 = \frac{1}{w-1} \sum_{s=t-w-1}^{t-1} \mathbf{y_{i,s}^2} \tag{8}$$

SW gives equal weight to all observations less than w time points in the past and 0 weight to all others. Removal of a highly influential outlying data point (that lies greater than 3 std. deviations) might cause a sudden change in the dynamic correlation that may be mistaken for an important aspect of brain connectivity. For this reason we applied auto-correlation filtering method on our data to make it smooth as possible to circumvent this issue. Also the purpose to compute this metric is to see if DCC was able to capture the correlation between the two time series at least to the level of SW from time points spaced at w-window width apart. Since, DCC is a very recent technique used in neuroimaging data analysis, we computed SW to also make

sure, the results computed by DCC are correct. Steps like these combined with simulation on data where we knew ground truth were critical as they helped us to improvise our research methods and select auto-correlation filtering technique as opposed to fermi-filtering we were using earlier.

Second step is the window selection process. A window length of 200 was chosen for our data based on experimentation. While it is beneficial to have a short window to better detect transient changes in connectivity, a large window is often necessary to allow for robust estimation of the correlation coefficient. (Lindquist, 2014)[8] Fig. 2 illustrates the effect of window length on the estimated conditional correlation fit to null data (i.e. two uncorrelated time courses). Note, that when using short windows, correlations are susceptible to large variations. In fact, a 95% confidence interval for null data will lie roughly between $\pm 2/\sqrt{w}$, which for a window length of 15 observations would roughly lie between [−0.5, 0.5]. Hence, using these settings random fluctuations can mistakenly be seen as meaningful time-varying correlations. The width of the 95% confidence interval is halved if we increase the window length four-fold to 60 observations. However, this comes at the cost of reduced sensitivity to minor changes in correlation.

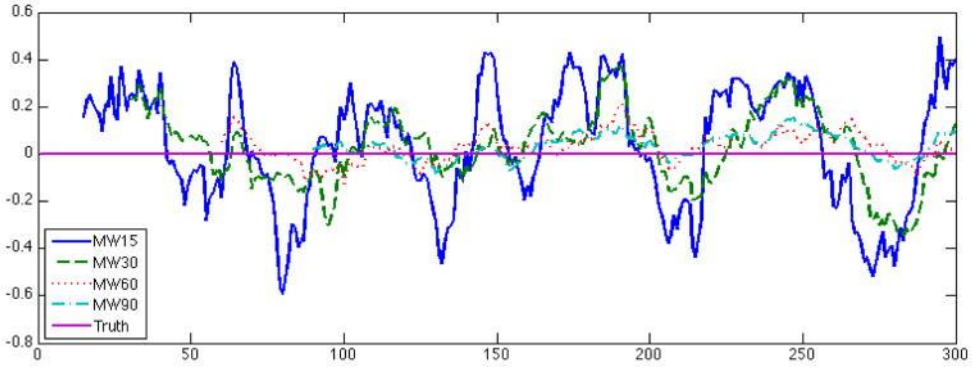

Figure 2. Various window sizes, 15-90 are used to estimate the ground truth. Largest window size, 90 appears closest to the ground truth and hence is a more robust estimate of dynamic correlation than smaller window sizes. (This simulation result is imported from Martin Lindquist[8])

2.3 MULTIVARIATE VOLATILITY MODELS

In this section we discuss two multivariate volatility models commonly used in the finance literature. The first, denoted the exponential weighted moving average (EWMA) approach, shares some similarities to sliding-windows. However, it provides solutions to some of the more obvious shortcomings of that approach. The second, the DCC model, provides a parametric approach towards estimating dynamic correlations, much like auto-regressive (AR) and auto-regressive moving averages (ARMA) models provide a parametric approach towards modeling fMRI noise (Purdon et al., 2001).

2.3.1 EWMA The first multivariate volatility model we introduce provides an alternative to the tapered sliding-window. The EWMA approach applies declining weights to past observations in the time series based on a parameter λ, and is based upon the following recursion

$$\Sigma_t = (1-\lambda)\boldsymbol{e}_{t-1}\boldsymbol{e}'_{t-1} + \Sigma_{t-1} \tag{9}$$

Where $\sum t$ is the conditional covariance matrix. This approach places the most weight on recent observations, and for each step away from *t* values become gradually down-weighted by a factor λ, before eventually being removed from further computations.

Decomposing the covariance matrix in Eq. 9, we can express the conditional variances and covariance as follows:

$$\sigma^2_{i,t} = (1-\lambda)\boldsymbol{e}_{t-1}\boldsymbol{e}'_{t-1} + \lambda\sigma^2_{t-1} \tag{10}$$

$$= (1-\lambda)\boldsymbol{y}_{i,t}\boldsymbol{y}'_{i,t-1} + \lambda\sigma^2_{t-1}$$

and

$$\sigma^2_{12,t} = (1-\lambda)\boldsymbol{e}_{1,t-1}\boldsymbol{e}'_{2,t-1} + \lambda\sigma^2_{12,t-1} \tag{11}$$

The parameter λ must take values between 0 and 1, and it determines how responsive the estimate of the covariance matrix is to the most recent time points. A small value of λ gives high weight to recent time points, while a large value produces estimates that respond more gradually

to new information. The value determines how many data points are included in the calculation and serves the equivalent purpose to the window size used in the sliding-window approach. Another important property of the approach is that as long as the recursion is initialized with a positive-definite matrix, it will remain so throughout the sequence.

Often the value of λ is set arbitrarily, with 0.94 being a popular value in the finance literature (Sheppard, 2012 [19]). However, if one assumes y_t to be bivariate Gaussian, it is straightforward to estimate λ through maximum likelihood estimation. Here, the log-likelihood function that should be maximized can be written:

$$\log\{L(\lambda)\} \propto -\frac{1}{2}\sum_{t=1}^{T}\|\Sigma_t\| - \frac{1}{2}\sum_{t=1}^{T}\boldsymbol{e}_t'\sum_{t}^{-1}\boldsymbol{e}_t' \tag{12}$$

This function can be maximized using any standard search algorithm and the value that λ takes at the optimum recorded.

Note, that as λ gets smaller, less of the past data is used in the calculation of the correlation. Hence, if one uses small values of λ one is susceptible to similar problems that arise when using short window lengths when computing sliding-window correlations. Hence, it is beneficial to estimate this important parameter directly from the data.

Finally, it should be noted that a related EWMA approach has previously been used to detect dynamic changes in the mean BOLD response (Lindquist et al., 2007). There the goal was

to detect so-called “change points” representing state-changes where the mean signal changes values, thus allowing one to model slowly varying processes with uncertain onset times and durations of underlying psychological activity. In contrast, this work considers dynamic correlations, which are perhaps more relevant for resting state analyses.

2.3.2 DCC Before discussing DCC, GARCH processes (Engle, 1982; Bollerslev, 1986), should be mentioned because DCC is a variant of multivariate GARCH processes. **GARCH that’s often used to model volatility in univariate time series, provides a flexible model for the variance in much the same manner that commonly used time series models, such as ARMA and AR, provide models for the mean.** GARCH models express the conditional variance of a single time series at time t as a linear combination of past values of the conditional variance and of the squared process itself. To illustrate, let us assume that we are observing a univariate process

$$y_t = \sigma_t \varepsilon_t \tag{13}$$

where ε_t is a N (0, 1) random variable and σ_t represents the time-varying variance term we seek to model. In a GARCH(1,1) process the conditional variance is expressed as

$$\sigma_t^2 = \omega + \alpha y_{t-1}^2 + \beta \sigma_{t-1}^2 \tag{14}$$

where $\omega > 0$, $\alpha, \beta \geq 0$ and $\alpha + \beta < 1$. Here the term α controls the impact of past values of the time series on the variance and β controls the impact of past values of the conditional variance on its present value.

If we set $\omega = 0$, $\alpha = 1-\lambda$ and $\beta = \lambda$, the GARCH(1,1) model expressed in eq. (14) can be written:

$$\sigma_t^2 = (1-\lambda)y_{t-1}^2 + \lambda\sigma_{t-1}^2 \tag{15}$$

which is equivalent to the EWMA model for the variance described in Eq. 10. Hence, though quite different in appearance, the GARCH(1,1) model provides a generalization of the EWMA model. While GARCH(1,1) processes are the most widely used in practice, there exist a more general class of GARCH(p,q) models. Here the p most recent observations of y_t^2 and the q most recent estimates of σ_t^2 are used in the updated estimates of σ_t^2. The model takes the form:

$$\sigma_t^2 = \omega + \sum_{i=1}^{p} \alpha_j y_{t-1}^2 + \sum_{j=1}^{q} \beta_j \sigma_{t-1}^2 \tag{16}$$

with $\alpha_1, \ldots \alpha_p, \beta_1 \ldots \beta_q \geq 0$, $w > 0$ and $\sum_{i=1}^{\max(p,q)}(\alpha_i + \beta_i)y_{t-i}^2 < 1$. While we include the general formulation for completeness, we note that models with large values of p and q may not be appropriate for fMRI data sampled at 2s time intervals, though with decreasing TR values they may become increasingly important.

While many multivariate GARCH models exist that can be used to estimate dynamic correlations, it has been shown that the DCC model out-performs the rest (Engle, 2002 [15]). To illustrate the DCC approach, again assume $\mathbf{y}_t = \varepsilon_t$ is a bivariate mean zero time series with conditional covariance matrix Σt. The first order form of DCC can be expressed as follows:

$$\sigma_t^2 = \omega_i + \omega_i y_{i,t-1}^2 + \beta_i \sigma_{i,t-1}^2 \text{ for } i = 1,2 \quad (17)$$

$$\boldsymbol{D}_t = diag\{\sigma_{1,t}, \sigma_{2,t}\} \quad (18)$$

$$\varepsilon_t = \boldsymbol{D}_t^{-1} \boldsymbol{e}_t \quad (19)$$

$$\boldsymbol{Q}_t = (1 - \theta_1 - \theta_2)\bar{\boldsymbol{Q}} + \theta_1 \varepsilon_t \varepsilon'_{t-1} + \theta_2 \boldsymbol{Q}_{t-1} \quad (20)$$

$$\boldsymbol{R}_t = diag\{\boldsymbol{Q}_t\}^{-1/2} \boldsymbol{Q}_t \, diag\{\boldsymbol{Q}_t\}^{-1/2} \quad (21)$$

$$\Sigma_t = \boldsymbol{D}_t \boldsymbol{R}_t \boldsymbol{D}_t \quad (5)$$

The DCC algorithm basically consists of two steps. In the first step (Eqs. 17–19), univariate GARCH(1,1) models are fit (Eq. 17) to each of the two univariate time series that make up $\mathbf{y}_t$, and used to compute standardized residuals (Eq. 19). In the second step (Eqs. 20, 21 and 5), an EWMA-type method is applied to the standardized residuals to compute a non-normalized version of the time-varying correlation matrix R_t (Eq. 20). Here represents the unconditional covariance matrix of ε_t and (θ_1, θ_2) are non-negative scalars satisfying $0 < \theta_1+\theta_2 < 1$. Eq.(5) is simply a rescaling step to ensure a proper correlation matrix is created, while Eq. 24 computes the time-varying covariance matrix. The model parameters (ω_1, α_1, β_1, ω_2, α_2, β_2, θ_1, θ_2) can be estimated using a two-stage approach. In the first stage, time-varying variances are estimated for each time series. In the second stage, the standardized residuals are used to estimate the dynamic

correlations. This two-stage approach has been shown to provide estimates that are consistent and asymptotically normal with a variance that can be computed using the generalized method of moments approach has been shown to provide estimates that are consistent and asymptotically normal with a variance that can be computed using the generalized method of moments approach.

Fig. 3 illustrates the estimated conditional correlation fit to null data (i.e. two uncorrelated time courses) using DCC. Clearly the method is able to closely follow the true value and appears to be a good candidate for use with fMRI data. Due to the parametric nature of the model, confidence bands can be created for the dynamic correlation term by using the first two moments of the DCC parameters to simulate their empirical distribution under the assumption of joint normality. Monte-Carlo methods can then be used to repeatedly draw from the estimated distribution of the coefficients, refit the model and create confidence intervals for the dynamic correlations.

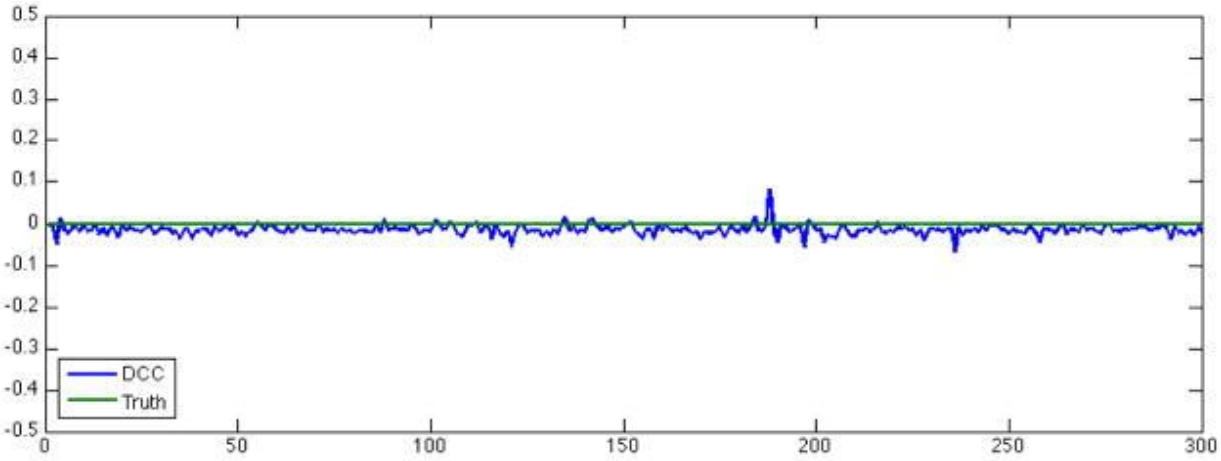

Figure 3. As we can see above, the DCC (dynamic conditional correlation) estimates (represented by blue line) are very close to the ground truth (green line). (This simulation result is imported from Lindquist et. el. 2014 [8])

3.0 EXPERIMENTAL SETUP

Optical-based neuro-imaging methods were used to concomitantly image low-frequency changes in neuronal as well as in hemodynamic signals. The fluctuations of the hemodynamic measurements were sensitive to blood oxygenation (analogous to fMRI measurements) and CBV (to assess vascular contributions). To see the correspondence between GCamp and OIS, healthy transgenic mice expressing GCaMP3, a fluorescent calcium indicator that reports changes in intracellular calcium concentration that accompany spiking activity (Chen et al., 2012)**[9]**, were used. GCaMP3 (or GCaMP) is widely expressed across the cortex, avoiding the use of point measurements (e.g., electrodes) or potentially toxic neural reporters (e.g., voltage-sensitive dyes), and therefore presents an ideal model to investigate the neuronal contribution to low-frequency hemodynamic oscillations.

3.1 GCAMP MICE

To understand how the cortex processes neural information, one must record the activity of large neuronal populations across large portions of cortical space. Ideally, one would monitor all the neurons in a cortical area to understand the underlying action potential map. However, even a single motor area event in the mouse cortex can be spread over many square millimeters.

Current techniques that record from distinct neurons—microelectrode arrays and two-photon imaging—cannot achieve this spatial coverage. Thus wide-field microscope-based optical imaging methods are suitable to measure the changes in neuronal activity and hemodynamic fluctuations in the brain over a large cortical surface in awake and anesthetized mouse. Since neuronal activity is closely coupled to intracellular calcium dynamics, calcium imaging has proven invaluable for imaging of neuronal activity. However, imaging with calcium sensors is not trivial. Traditional bulk-loading of calcium sensors only last for periods of hours, making chronic recordings of neuronal activity over extended times difficult. Genetically encoded calcium indicators overcome many of these limitations. GCaMP3 is a genetically encoded calcium indicator, (or GECI) that has certain advantages over the conventional dyes: (1) in species with a thin cranium, such as mice, they allow for noninvasive imaging; (2) they allow genetic targeting to specific cell populations, providing a handle into cellular diversity; (3) they provide reliable recordings, from those cell populations over prolonged periods and multiple sessions; and (4) they enable transgenic expression strategies for highly reproducible delivery of the indicator (Matteo Carandini et. el. 2015 [20]). However, like most indicators, GECIs have optical spectra that overlap with the absorption spectrum of hemoglobin (Hillman, 2007[21]). The intensity of their fluorescence measured through blood-perfused tissue, therefore, is corrupted by vascular signals. These signals reflect changes in local blood volume and oxygenation that are associated with heart beats and with hemodynamic responses. The latter are particularly large and fast during wakefulness (Pisauro et al., 2013 [22]), thus posing a considerable challenge. In the coming chapters we will focus on processing these slow fluctuations captured by these optical imaging methods, under these challenging environments, to correctly interpret and compare the neural and hemodynamic response.

While multiple analysis techniques exist to look at the dynamics of time-series data, the most commonly used are the region-of-interest (ROI) based analysis and the independent component analysis (ICA). The first is based on the extraction of the time-course of the BOLD signal from a pre-defined ROI and subsequent identification of the regions showing a significant correlation with the ROI. This time-course correlation analysis produces functional connectivity maps showing which areas are connected with the given ROI and to what extent. This method represents the most straightforward way to study the functional connectivity, as the results are relatively clear and simple to interpret. ICA, by contrast, is a statistical technique that does not involve any a priori assumption and allows the exploration of multiple whole-brain networks.

3.2 ANIMAL PREPARATION (VAZQUEZ ET. EL. 2014)[7]

Seven adult transgenic mice expressing GCaMP3 throughout the central nervous system were used for this study. This transgenic strain contains the thymus cell antigen 1 (Thy1) promoter driving expression of an eGFP-calmodulin fusion protein, GCaMP3 in the entire central nervous system. Specifically, GCAMP3 is expressed in cortex, hippocampus, thalamus, cerebellum, superior colliculus, amygdala, brain stem, retina and spinal cord. An increase of green fluorescence in specific neurons can be observed as the result of elevated intracellular calcium. In these GCaMP3 mice, cytoplasmic fluorescence is evident in the somata of layer V and layer II/III neurons of the living cortex, and in glomerular and mitral cell layers of the olfactory bulb.

GCAMP expression is higher in these mice than in B6;CBA-Tg(Thy1-GCamp2.2c)8Gfng/J mice. GCaMP3 mice allow fluorescent detection of activated neurons at the cellular level. All procedures performed followed an experimental protocol approved by the University of Pittsburgh Institutional Animal Care.

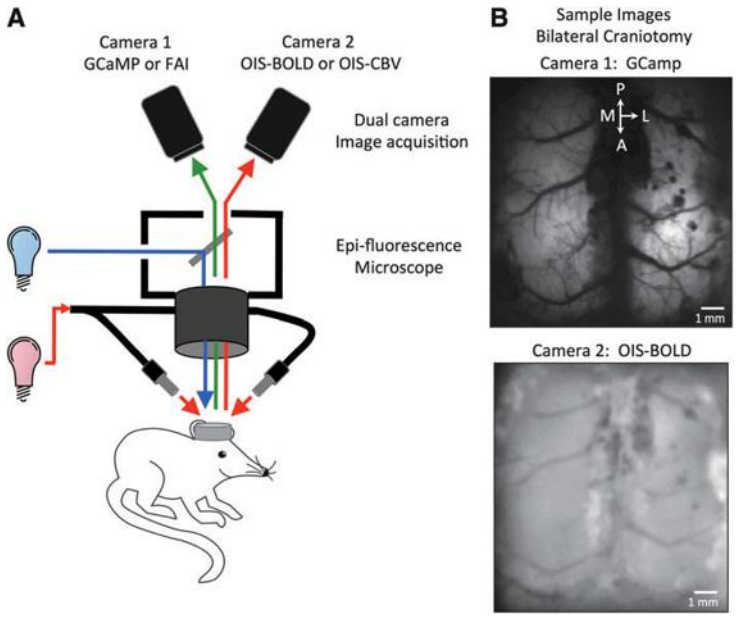

Figure 4. A. Shows experimental setup used to image the cortical surface of GCAMP3 mouse. Microscope was used to focus on a large field of view on the mouse such that the exposed part of its brain after surgery is captured using two cameras (Camera 1 was used for GCaMP imaging used to capture neuronal activity on mouse's cortical surface. Simultaneous image capturing was performed by camera 2 that collected OIS-BOLD and OIS-CBV data from the microscope's output image. B. The sample images captured by both camera are shown; GCaMP on top and OIS-BOLD at the bottom.)

The animals were initially anesthetized using a cocktail of ketamine (75 mg/kg) and xylazine (10 mg/kg). The drug was administered intraperitoneally (IP) for surgery. An IP line was then inserted to administer fluids with 5% dextrose in saline as well as supplementary anesthesia throughout the experiment. The animals were then placed in a stereotaxic frame (Narishige, Tokyo, Japan) and supplementary oxygen was administered blow-by using a cannula at a rate of 500 mL/min. Heart rate was continuously monitored throughout the experiment using metal leads placed subcutaneously in the abdomen to assess the physiological condition of the animal and depth of anesthesia. Body temperature was maintained at 38℃ using a thermal probe and heating pad controlled by a DC feedback unit. The thermal probe was placed under the abdomen to maintain the animal's temperature throughout the experiment. Heart rate and body temperature were recorded using a polygraph data acquisition software (Acknowledge; Biopac Systems, Inc., Goleta, CA). The skull was then exposed over both hemispheres. A well was made using acrylic cement surrounding an area about 9 ·7mm2, centered about 1mm posterior to Bregma. The skull in this area was then removed using a dental drill. The well area was then filled with 1% agarose gel at body temperature. At least 15 min was allotted for the setup to settle prior to commencing experimental data collection.

3.3 NEURAL IMAGE ACQUISITION

Paragraph. GCaMP and OIS-BOLD as well as the GCaMP and OIS-CBV images were recorded simultaneously from all GCaMP mice using these light-splitting optics shown in Figure 4. Images sensitive to neuronal activity were acquired from GCaMP mice using an epifluorescence

microscope (MVX-10; Olympus, Tokyo, Japan) over a field-of-view of 11.9 ·8.9mm2 (Fig. 4). GCaMP was excited using a mercury lamp light source coupled to a low-noise power supply (Opti-Quip, Highland Mills, NY) and an appropriate excitation filter (470 – 20nm). The fluorescence emission over 525 –25nm was captured using a digital-cooled CCD camera (Cool-Snap HQ2; Photometrics, Princeton, NJ) at a frame rate of 10Hz in 5-min recording periods. The exposure time of the camera was set to 100msec with a bin factor of 3 to increase signal-to-noise ratio (SNR) for an effective pixel resolution of 26 lm. The same microscope and optical path were used for simultaneous optical imaging of intrinsic signal (OIS) sensitive to either blood oxygenation (OISBOLD) or CBV (OIS-CBV) (for all animals) (Fig. 4).

Oblique light guides, transmitting filtered light of 600– 50nm, were connected to a halogen light source (Thermo-Oriel, Stratford, CT) and were used for illumination. Corresponding isobestic point for hemoglobin, a barrier filter of 572 ± 7 nm was placed prior to the camera for OIS-CBV. Since the light range corresponds to an isosbestic point for hemoglobin, the acquired images were sensitive to hemoglobin measurement and quantification. Thus, the images are representative of CBV. A barrier filter, corresponding to a spectral region dominated by deoxygenated hemoglobin light absorption, between 620 ± 7 nm was similarly placed for OIS-BOLD. The OIS data were acquired at 30Hz using an analog CCD camera (Sony XT-75, Tokyo, Japan) and an analog-to digital frame-grabbing board (Matrox, Inc., Dorval, Quebec, Canada) over the same field-of-view. The OIS pixel size was 14 μm.

3.4 IMAGE PROCESSING & DATA PROCESSING PIPELINE

The images were first motion corrected to correct for breathing induced motion in mice. In-house image registration method (using MATLAB, Mathworks library) was applied using a two-dimensional rigid body model with two degrees of freedom (x- and y translations). The SNR of the data was increased by binning the GCaMP images by a factor of 2 and the OIS images by a factor of 4 for a final in-plane pixel resolution of 52 and 56 μm, respectively. In addition, the OIS data were temporally binned by a factor of 3 to match the sampling rate of the GCaMP and FAI data (10 Hz).

Skull-stripping was performed by regressing the bone from the images. To focus on neural activity, specifically, the changes we want to observe and to extract unwanted fluctuations in the light source, an average of time-series was subtracted from each image. In our earlier research endeavors, the data were band-pass filtered from 0.02 to 0.2 Hz in frequency domain using a Fermi filter with spread parameter of 0.005 and 0.05 Hz at each band, respectively, to maintain low-frequency fluctuations while removing bulk baseline drifts (Vazquez et. el. 2014)**[7]**.

A k-means algorithm was then used to outline six clusters from one hemisphere (typically the left hemisphere) based on the correlation distance between the pixel's time series for each imaging data set. K-means is an unsupervised iterative algorithm that partitions a given set of data-points, and in our case, the neural activity/hemodynamic fluctuations in pixels, into a pre-specified number of clusters. The number of clusters was chosen to be 6 for mice cortex. This number is based on a previous report on the number of identifiable areas over the superior surface of the mouse brain (White et al., 2011)**[6]**. 6 (k=6) centroids, one for each cluster, are

placed randomly on the cortical surface. Each pixel belonging to a given GCamP 2D image was then associated it with the nearest centroid. At this point we re-calculate 6 new clusters (thus 6 new centroids) using the centroids of the clusters resulting from the previous step.

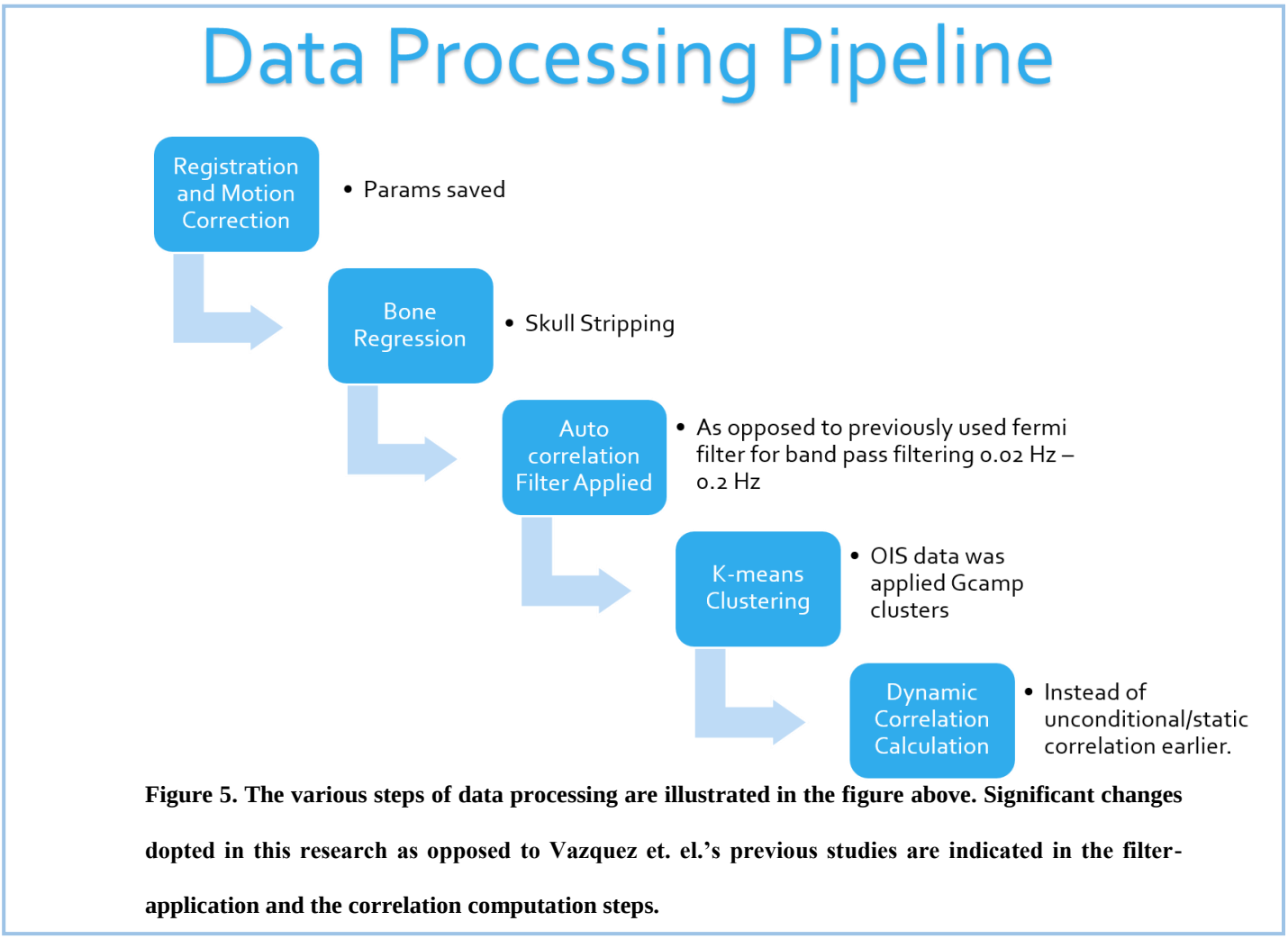

Figure 5. The various steps of data processing are illustrated in the figure above. Significant changes dopted in this research as opposed to Vazquez et. el.'s previous studies are indicated in the filter-application and the correlation computation steps.

To solve this loop, where we find the centroid for the 6 clusters that befits the data points, the *objective function*, is minimized.

The objective function:

$$J = \sum_{j=1}^{k} \sum_{i=1}^{n} \left\| x_i^{(j)} - c_j \right\|^2 ,$$

where $\left\| x_i^{(j)} - c_j \right\|^2$ is a chosen distance measure between a data point $x_i^{(j)}$ and the cluster centre c_j, is an indicator of the distance of the *n* data points from their respective cluster centres.

For this, the distance matrix is the correlation. Distance correlation is a measure of dependence between random vectors. Given an m-by-n data matrix X, which is treated as m (1-by-n) row vectors x1, x2, ..., xm, the correlation distances between the vector xs and xt are defined as follows:

$$d_{st} = 1 - \frac{(x_s - \bar{x}_s)(x_t - \bar{x}_t)'}{\sqrt{(x_s - \bar{x}_s)(x_s - \bar{x}_s)'}\sqrt{(x_t - \bar{x}_t)(x_t - \bar{x}_t)'}}$$

In our previous research endeavors both GCaMP and OIS data were processed individually to obtain the 6 clusters (Vazquez et. el. 2014**)[7]**. However, for this research, we chose a 2D GCaMP image and applied k-means clustering on it, then applied the resultant ROIs (clusters) to all GCaMP and OIS time-series of all animal data. By selecting regions, correlation-wise closest to each other, we reduced the large number of pixel-wise time series into a finite and small number of time series. Thus, we simplified the computational problem to computing correlation between any two ROI time series. Distinct and contiguous clusters were consistently

obtained over anatomical areas that approximately correspond to cingulate, frontal, motor, somato-sensory, retrosplenial, and visual cortices.

1) **Comparison at a glance GCAMP vs. OIS**

GCAMP Data	OIS Data
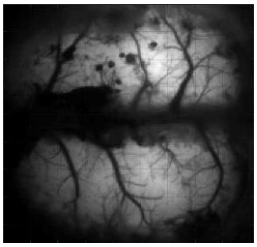	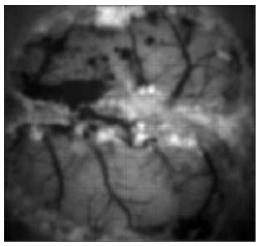
Technical Specifications : - The size of this image is 173 x 165 - Intensity values vary from 127 to 2300 and above. - Contrast between the cortical surface and the surrounding region is high, in short SNR is high. - The blood vessels and the region around cortical surface is dark.	Technical Specifications : - The size of this image is 154 x 164 - Intensity values vary from 80 to 517 - Contrast between the cortical surface and the surrounding region is lower, in short SNR is lower. - This needs contrast adjustment. - The blood vessels and the region around cortical surface is overall dark but we can see artifacts of blight light.

homocorOIS Filter Applied Over all both GCAMP and OIS data look very similar to each other, except:	
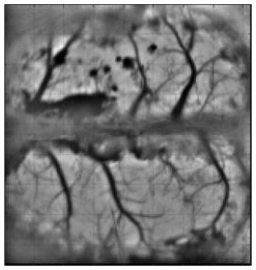	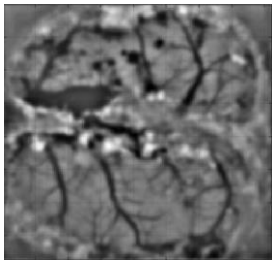
- The data looks very good. - SNR is good - The gradient between the data and the background is smooth.	- Data looks mixed with background in the central fissure. - The bright spots look more prminant - The gradient between the data the background is very abrupt→ large.

Figure 6. Comparison of GCaMP data (that reflects the neuronal changes) and the OIS-BOLD (hemodynamic fluctuations) is shown

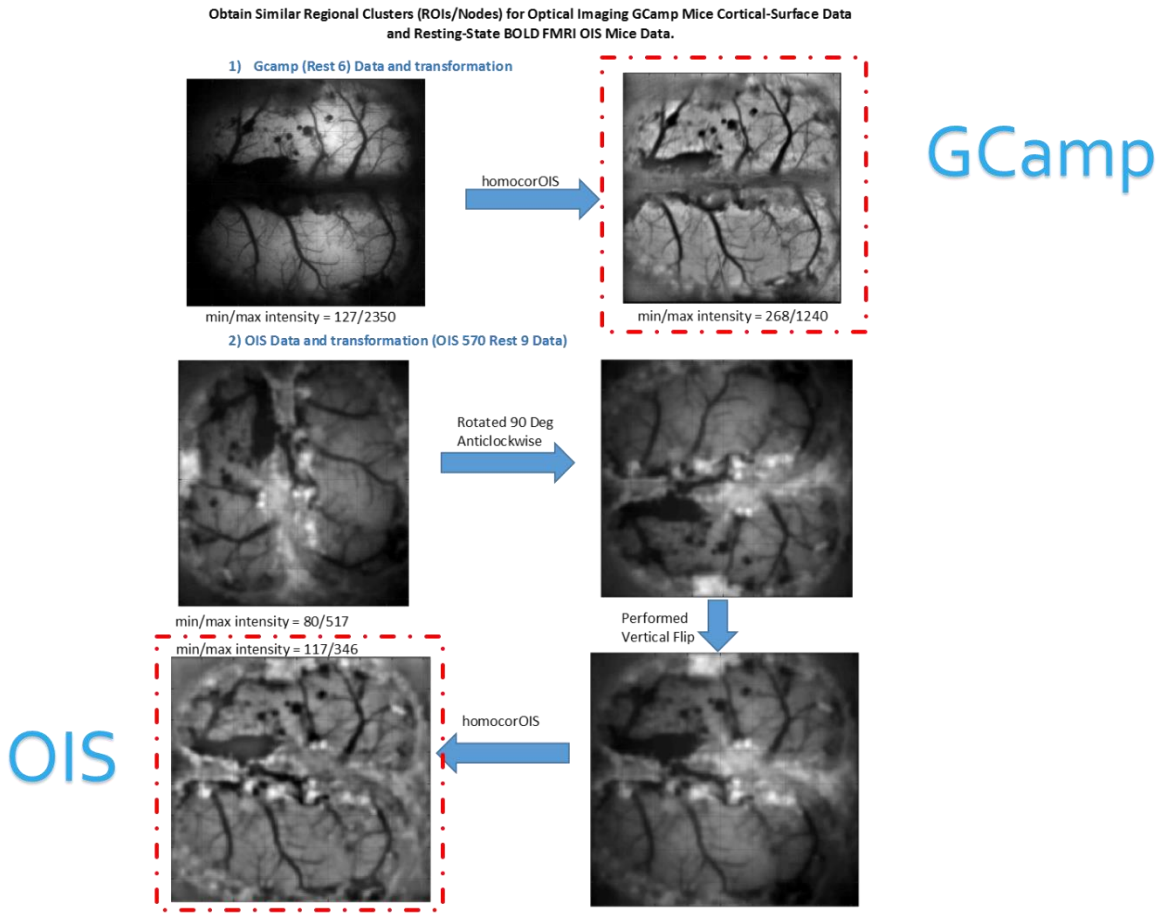

Figure 7. Differences between GCaMP and OIS data. Some image manipulation before motion correction is applied for effective removal of motion effects in the images due to mouse's breathing.

Moreover, by comparing the mean intensity value of an ROI (also called as node), with another, we get a correlation value that represents the degree of similarity between the two regions.

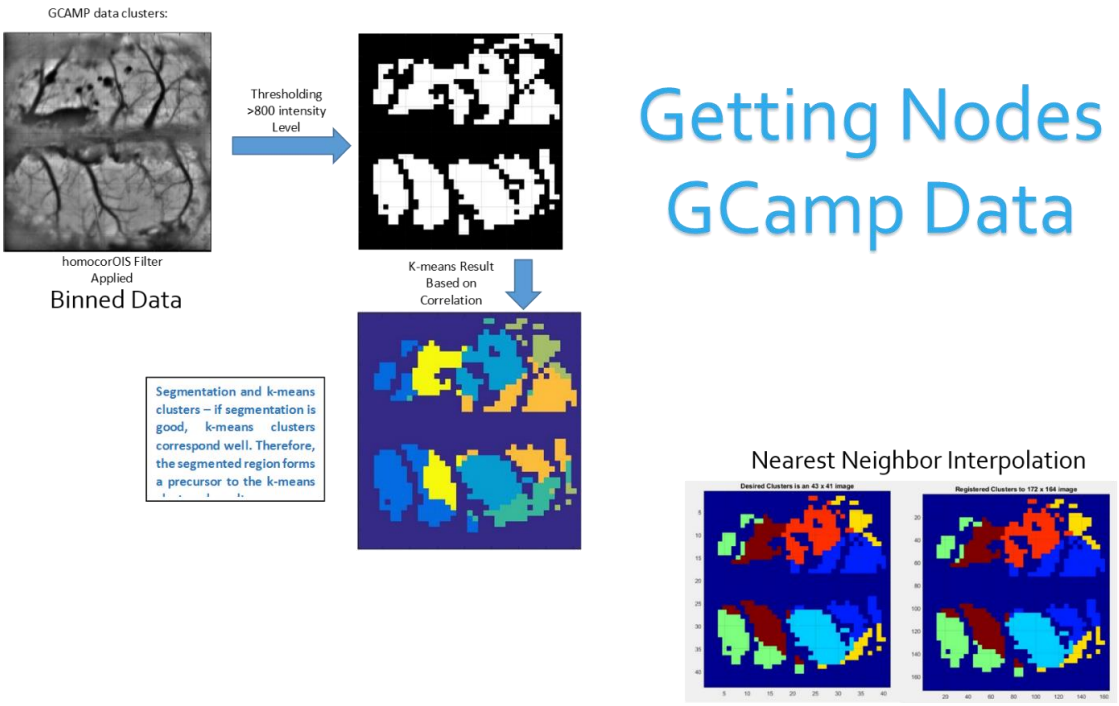

Figure 8. K-means application on GCaMP image to obtain spatially correlated 6 ROIs. K-means clustering was applied on an image with larger bin number than the image used for processing data. To fit these clusters on the data, nearest neighbor interpolation was applied.

Connectivity correlation: The connectivity matrix (6 · 6) for the GCaMP, OIS-BOLD, and OIS-CBV data was calculated using the cluster average time series from each respective imaging modality while holding the spatial extent of the clusters constant. The GCaMP cluster map was chosen as the standard of reference because of its sensitivity to neuronal activity. The connectivity correlation was then calculated as the correlation between corresponding off-diagonal connectivity matrix elements obtained from the GCaMP and OIS data. Since the

connectivity matrix is symmetric along its diagonal, only the upper-triangular elements were used.

In our previous research, where we explored the degree with which hemodynamic connectivity was associated with neuronal, metabolic, and vascular connectivity measures, the following metrics were generated to investigate correspondence between neural and hemodynamic connectivity based on blood-oxygenation- and CBV-sensitive OIS data. The connectivity correlation metric was used as an indication of the accuracy the hemodynamic data (OIS) was in indicating neuronal connectivity (GCaMP). The significance of this relationship was determined using a paired t-test with $p < 0.05$ for each animal. The results showed that there was a significant agreement (strong connectivity correlation) between the two as shown in Table 1. The overall correspondence of the connectivity-cluster maps across modalities was generally good although some deviations were observed in all animals. The network clusters calculated using either GCaMP or OIS-BOLD data exhibited high and significant connectivity correlation. And we concluded that the blood-oxygenation-based hemodynamic connectivity was a valuable surrogate for the underlying neuronal connectivity. (Vazquez et. el. 2014**)[7]**

For fMRI analysis, a common practice is to assume that the functional connectivity (FC) between time series from distinct brain regions is constant across time. Recently, there has been an increased interest in attempting to quantify the dynamic changes in FC during the course of an fMRI experiment, particularly during resting state. Also, it is worth noticing that the correlation metric we used for our previous study is not based on any previous (on temporal-axis) information and thus it is called as unconditional correlation. However, in light of “dynamic” changes present in the data, the mean and the variance of this data over the time series are not

constant. Thus the unconditional metrics, such as conventional statistical correlation methods are rather insufficient for adjudging correlation between the non-stationary or dynamic signals.

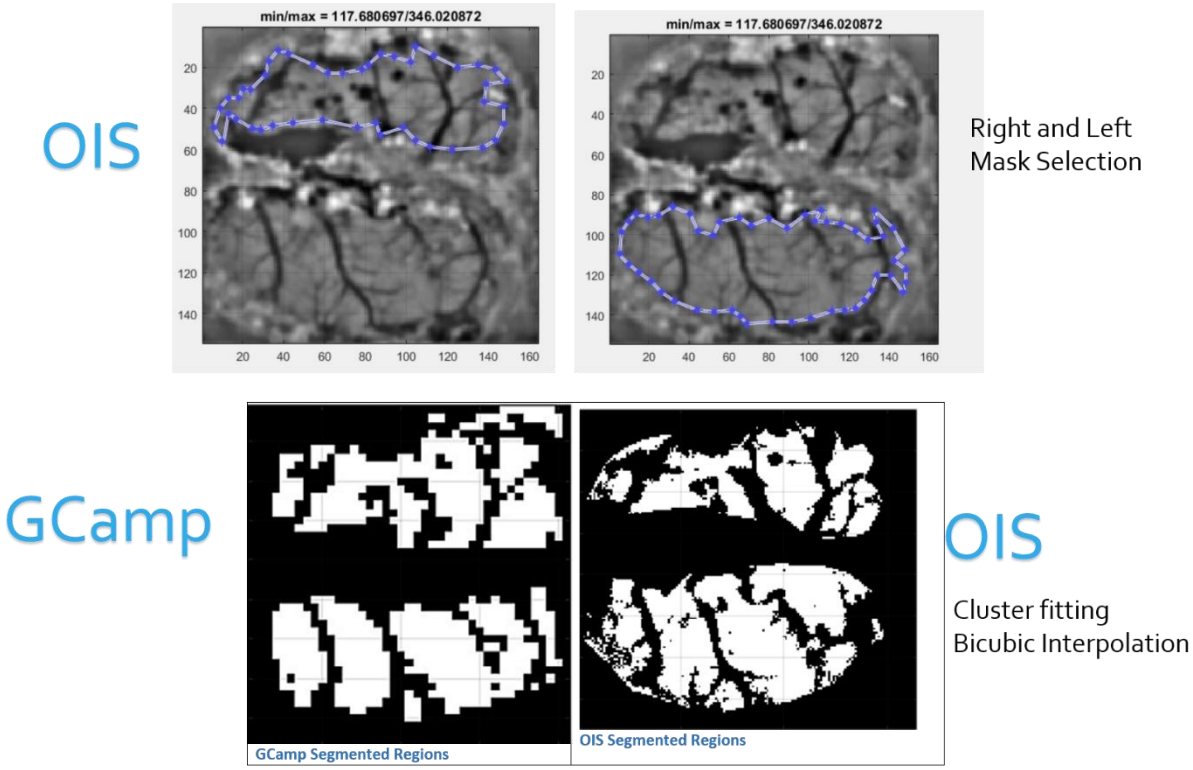

Figure 9. Mask selection process shown on OIS data. The clusters obtained from the GCaMP data were applied on the OIS data where masks were pre-selected interactively. This scheme was applied on all images in the time-series. At the right bottom, we can see clus clusters on the OIS image. In both GCaMP and OIS clustered images, we have stripped the skull and removed blood vessels. Only the cortical surface is used for our analysis.

Table 1. Previous Results: Connectivity Correlations Obtained from all Animals Studied

Comparison	Connectivity Correlation
GCaMP vs. OIS-BOLD	
GCaMP mouse 1	**0.958***
GCaMP mouse 2	**0.775***
GCaMP mouse 3	**0.750***
GCaMP mouse 4	**0.581***
GCaMP mouse 5	**0.811***
GCaMP mouse 6	**0.779***
GCaMP mouse 7	**0.801***
Average – SD	0.780 – 0.111

3.5 FILTER SELECTION - SIMULATION

In our previous studies (Vazquez. et. el. [7]), we have shown that low-frequency (<0.1 Hz) changes at neuronal and hemodynamic level measured using microscope and recorded using camera while the brain is in resting state (i.e., not performing any task), show specific bilateral patterns that outline known connectivity within brain networks. There was significant level of correlation between the two modalities; at neuronal and hemodynamic level as shown in Table 1. To obtain low-frequency range from the available signal, we applied fermi filter on our acquired

data. For our analysis, we observed cortical surface of the brain over a period of 5 minutes each at 10 Hz sampling rate. The recorded brain-images thus represent a collection of 2D image-data acquired over this time period. The product of the rows and columns of the 2D image is the total number of variables, each generating 1D time series signal, is our computational challenge that we want to analyze and study. Thus the data represents a multivariate time-series where each variable, mapping the maximally resolvable region on the brain surface, represents a univariate time-series or a 1D signal. One of the main goals of time-series analysis is to identify the nature of phenomenon (in our case to study the resting state processes) represented by the sequence of observations. Thus a fermi filter of 0.02 – 0.02 Hz was applied. This method worked out well for our previous analysis, however, it fell short for our current analysis. We will first showcase what went wrong while processing the real GCAMP (camera captured neuronal activity) and OIS (camera captures hemodynamic activity) data in order to describe the rationale behind changing the filter. Then we will proceed to describe the simulation where we selected the appropriate filter such that the results matched what the visual results showcased. It's important to mention that a signal whose spectrum matches the random noise's provides compatibility with DCC computation. Since fermi filter did not alter the decay function, from common knowledge, AR filters should work to provide us z-transform information for GARCH models to compute conditional correlation more effectively. Fig 10 on left shows GCaMP image with neural activity (proportional to mage intensity). Fig 10 on the right shows two nodes classified earlier (by k-means), we can see one node is dark while the other is bright. This image was captured at a random time point out of 3000 time points in a 5 minute movie captured at 10 Hz sampling rate. This is good capture (image or frame) to demonstrate the method we used for eye-balling images in the time-series to see approximately, if the nodes (ROIs) were correlated, anti-correlated or uncorrelated. If both the regions were dark, i.e, the average pixel intensities was equal to zero then the nodes were uncorrelated. Conversely, if both were bright then they

were highly correlated with maximum value of 1. Consequently, when one was bright while the other dark, they were anti-correlated with the minimum possible value of -1. The idea was to see if the correlation values obtained using DCC was representing this relationship.

To make the process of correlation evaluation simpler we plotted the difference between the two nodes (1 and 4) with respect to time and plotted the values of DCC to see correspondences between the two. In Figure 11, the figure on top shows the plot of difference between the values (average intensity values) of the two nodes (ROIs, clusters) 1 and 4 as a function of binned time (by a factor 10) on the x-axis. Figure on the bottom shows DCC correlation values between the same nodes (1 and 4). We can see that there are issues with the values obtained. Since, DCC has been shown in several literatures to have worked well on this type of data (Lindquist, 2014 [8]), thus it got us thinking what could be the quantity that was not adding up.

The first problem we consistently noted with all animal data was, the values of DCC were varying between -1 and 1 sharply and in some cases the uncorrelated values of 0 were missed. The accuracy for which DCC is well-known (as shown in the simulation plots in Fig. 3) was missing. Thus, for application of conditional correlation methods on our time-series to analyze the similarity between the two modalities, it was important to find out the right type of filter for the data. To save time in data processing, we generated simulated GCaMP signals by adding Gaussian noise, 1/f noise to trapezoid signals of arbitrary duration, amplitudes and number of peaks. After application of the autocorrelation filter, we found out that the DCC and SW both performed very well on the data and provided correspondences in time points.

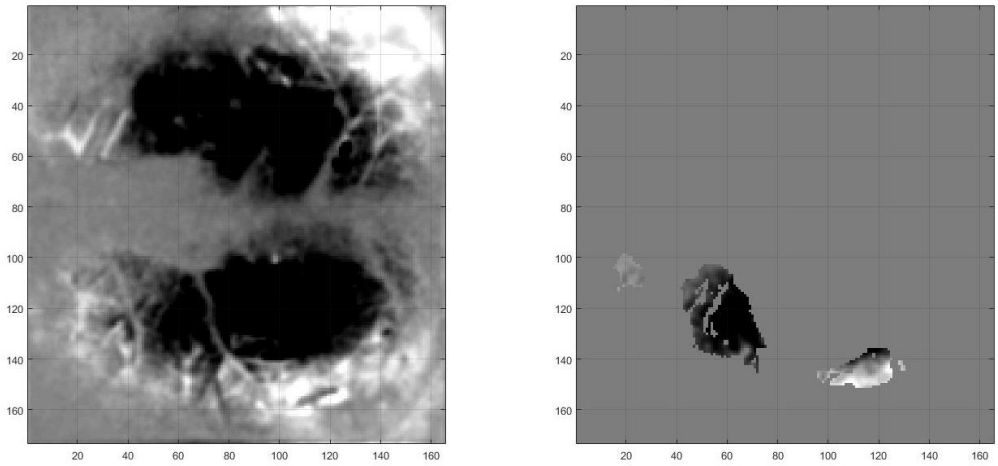

Figure 10. Figure on left shows GCaMP image with neural activity. Image intensity is the measure of the level of neural activity here. Figure on the right shows two nodes or ROIs clustered earlier (by k-means). As we can see one cluster is dark while the other is bright. This image was captured at a random time point out of 3000 time points in a 5 minute movie captured at 10 Hz sampling rate.

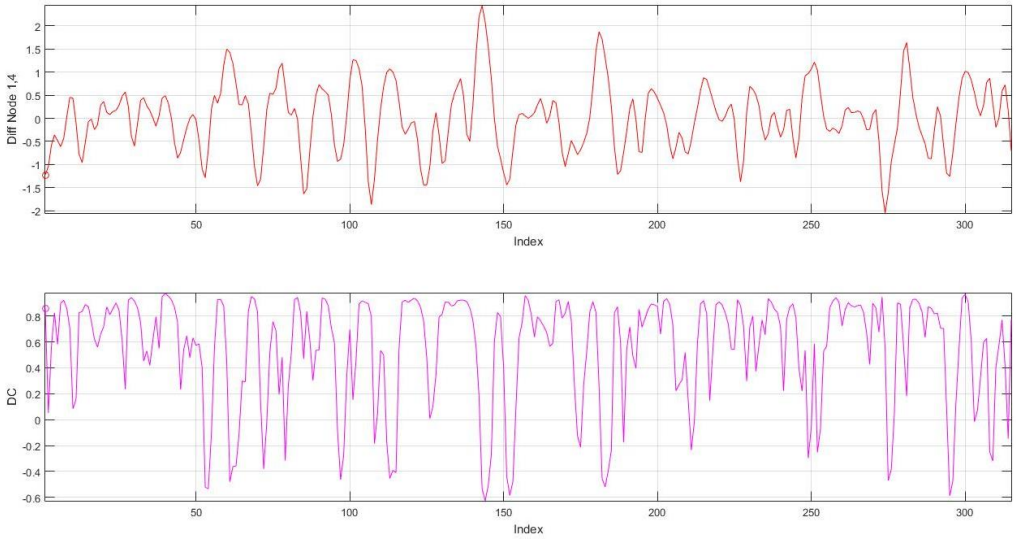

Figure 11. Figure on top shows the plot of difference between the values (average intensity values) of the two nodes (ROIs, clusters) 1 and 4 as a function of binned time (by a factor 10) on the x-axis. Figure on the bottom shows DCC correlation values between the same nodes (1 and 4).

Since, the spectrum of biological data looks like the spectral response in Fig. 15 (green plot), y = a/f, where the variable, a being constant and the variable f, which is the signal's spectrum, serves as the exponential decay function, we generated a simulated GCAMP function. We plotted trapezoid waves with arbitrary values of amplitude ranging between -5 to +5. Since the signals are of low frequency, the duration of wave was chosen to accommodate <0.1 Hz signal. No. of peaks was also selected randomly. To mimic the signal with 1/f decay (as shown in Fig. 15), we added this component to the signal. Figure 12 shows the trapezoid function (signal) in blue while the same signal added with 1/f component to make it (red) look like GCAMP signal. Signal was whitened (white noise was added), such that it looked like the real biological signal. To study the dynamic correlation between two simulated nodes, thus we created two such simulated GCAMP signals as shown in Fig. 14.

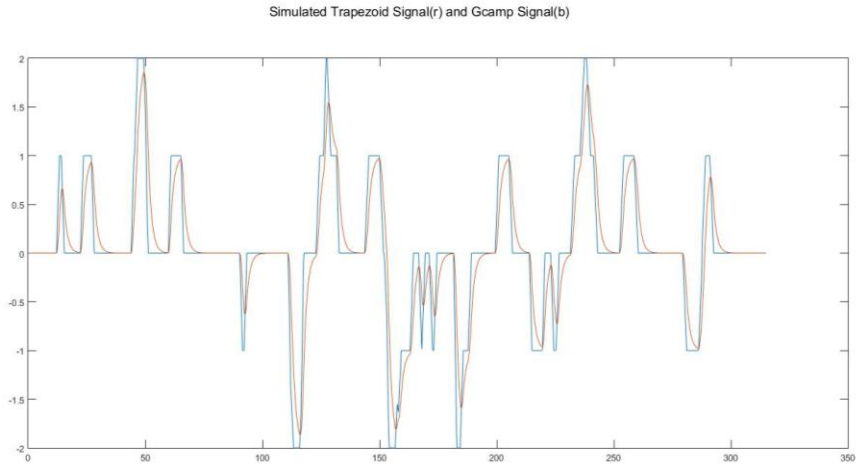

Figure 12. Figure shows the trapezoid function (signal) in blue while the same signal added with 1/f component to make it (red) look like GCAMP signal. (The figure above shows binned (by factor 10) time points on the x-axis from 0 to 300 for the 5 minute movie sampled at 10 Hz. The y-axis show the values of amplitudes of the respective signals.)

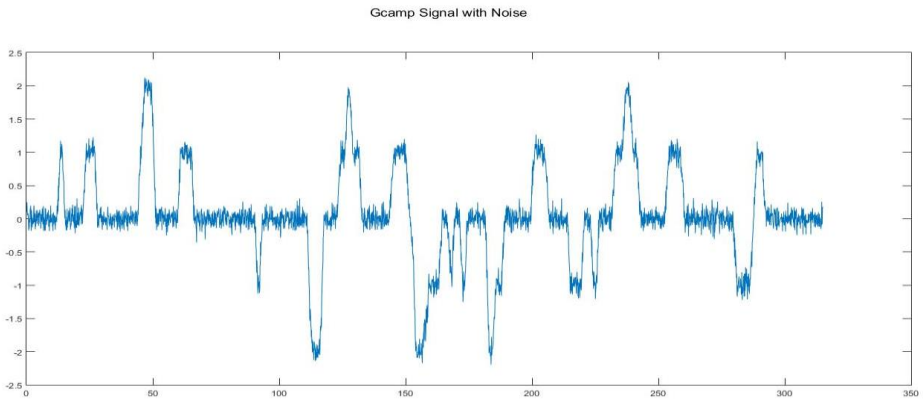

Figure 13. In addition to signal simulation in fig. 12, the signal was whitened (white noise was added), such that it looked like the real biological signal. (The figure above shows binned (by factor 10) time points on the x-axis from 0 to 300 for the 5 minute

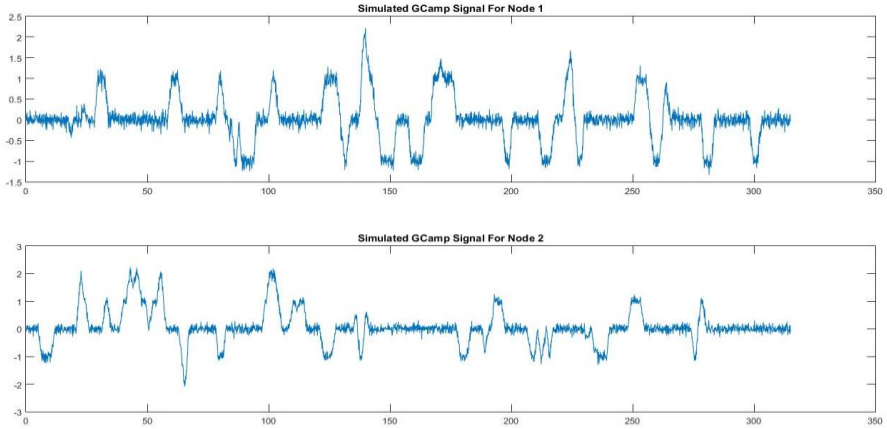

Figure 14. To study the dynamic correlation between two simulated nodes, thus we created two such simulated GCAMP signals. The figure above shows binned (by factor 10) time points on the x-axis from 0 to 300 for the 5 minute movie sampled at 10 Hz. The y-axes show the values of amplitudes of the respective signals.)

When we apply a band pass filter such as fermi filter, then the spectrum doesn't alter (red), as we can see in Fig. 15, just the frequencies we are interested in remain rest are filtered out. However, on using Auto-regressive (AR) filter, using Burg's method in built in MATLAB (Yule method can also be used), that works as a divided difference approach removed the 1/f component of the biological GCAMP signal spectrum, rendering the filtered spectrum of the GCaMP signal flat (blue spectrum in the Fig. 15). The use of AR filters has been shown to have work in synergy with the conditional correlation methods such as DCC and SW. On the time series, the difference between the fermi filter and the AR filter application can be appreciated in the Fig. 16 and 18. While fermi filter smoothed out the simulated data (2^{nd} plot from top Fig. 16), the divided differences approach of AR filters created a level-set for the simulated data (3^{rd} plot from top in Fig. 16). In figure 17, we can see the results of simulation and correlation computation. The first two plots from top are the simulated GCAMP signals. Plot 3 is the pearson correlation of the two signals, as a measure to approximately adjudge the values of DCC at the time points. The plot 4 is DCC computation while the fifth plot is the SW computation. Within this graph of unfiltered signals itself, on comparing the Pearson correlation values with DCC and SW, we can see that we fail to obtain uncorrelated values. This problem is more pronounced in the fermi filtered signals (Fig. 19, plots no. 3 and 4) where zero correlation was never achieved and the conditional correlation metric, DCC oscillated between the two extreme values frequently. However, we can see in Fig. 18 (plots 3 and 4), that AR filtered signals work much better with DCC and SW. We do achieve the correlation values that we set out to observe with the real data. Thus our simulation results indicated that the simulated GCAMP signals when treated with AR filter resulted in better performance of the conditional correlation methods.

Consequently, we processed our real data with AR filter before application of both DCC and SW.

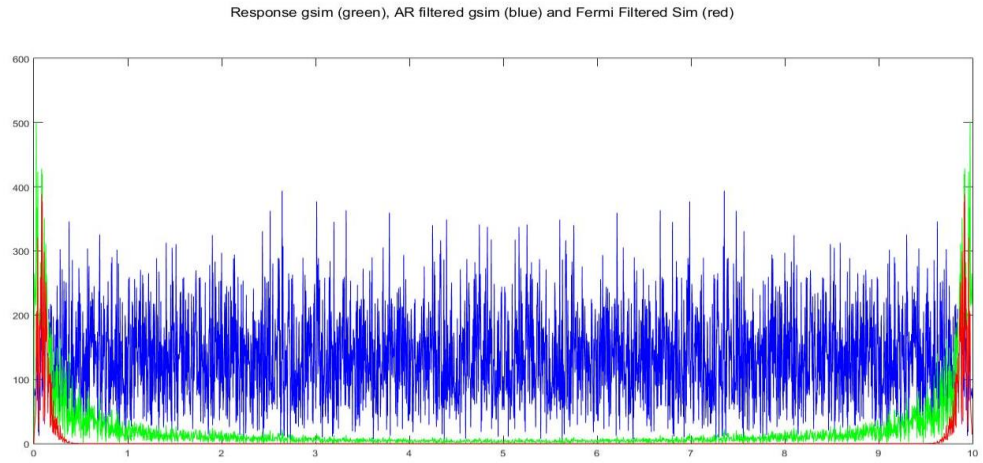

Figure 15. Frequency response of biological signal (GCaMP mice) shown in green. we can see that the spectral analysis of GCAMP signal (green plot) shows a decay at low frequencies (<1 Hz).

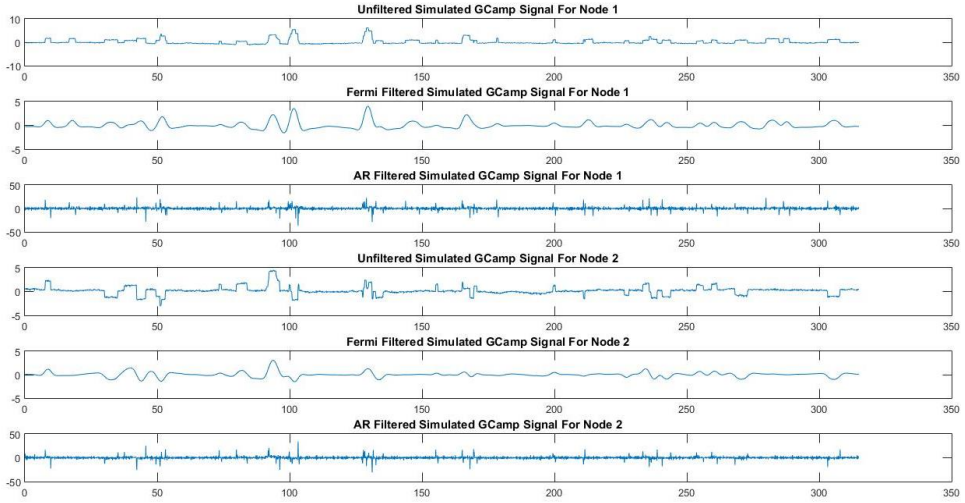

Figure 16. This figure shows the Fermi and AR filter application on the simulated GCAMP signal. The figure above shows binned (by factor 10) time points on the x-axis from 0 to 300 for the 5 minute movie sampled at 10 Hz. The y-axes show the values of amplitudes of the respective signals.

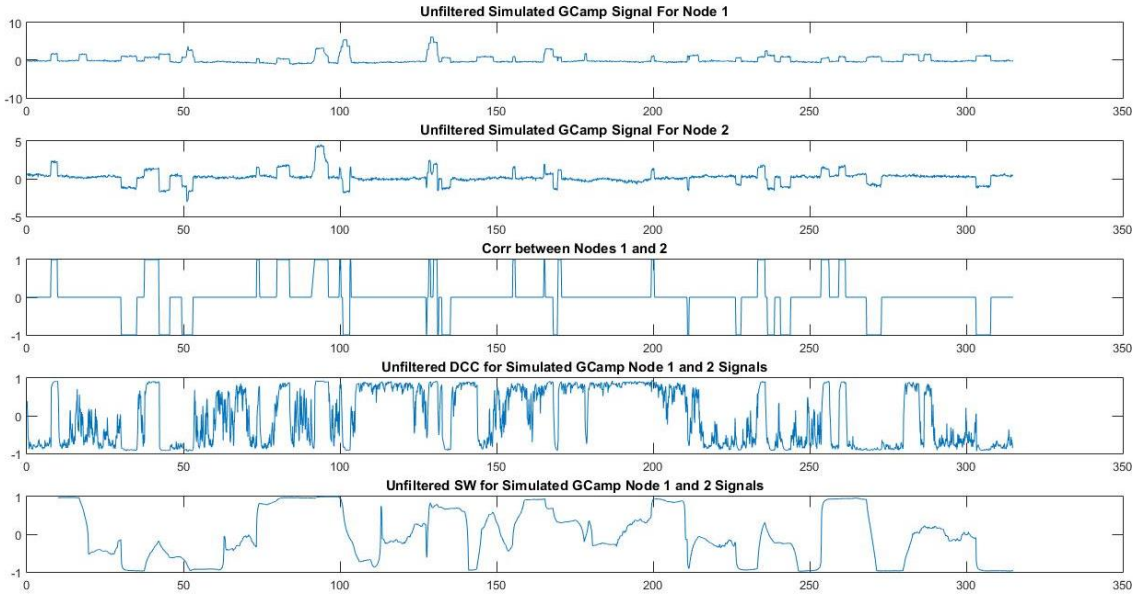

Figure 17. We can see the results of simulation and correlation computation on unfiltered simulated signal. The first two plots from top are the simulated GCAMP signals. The third plot is the pearson correlation of the two signals, as a measure to approximately a adjudge the values of DCC at the time points. The fourth plot is DCC computation while the fifth plot is the SW computation. (The figure above shows binned (by factor 10) time points on the x-axis from 0 to 300 for the 5 minute movie sampled at 10 Hz. The y-axes show the values of amplitudes of the respective signals for the top two figures and the values of correlation coefficient, ranging between -1 to 1, for the bottom three figures.)

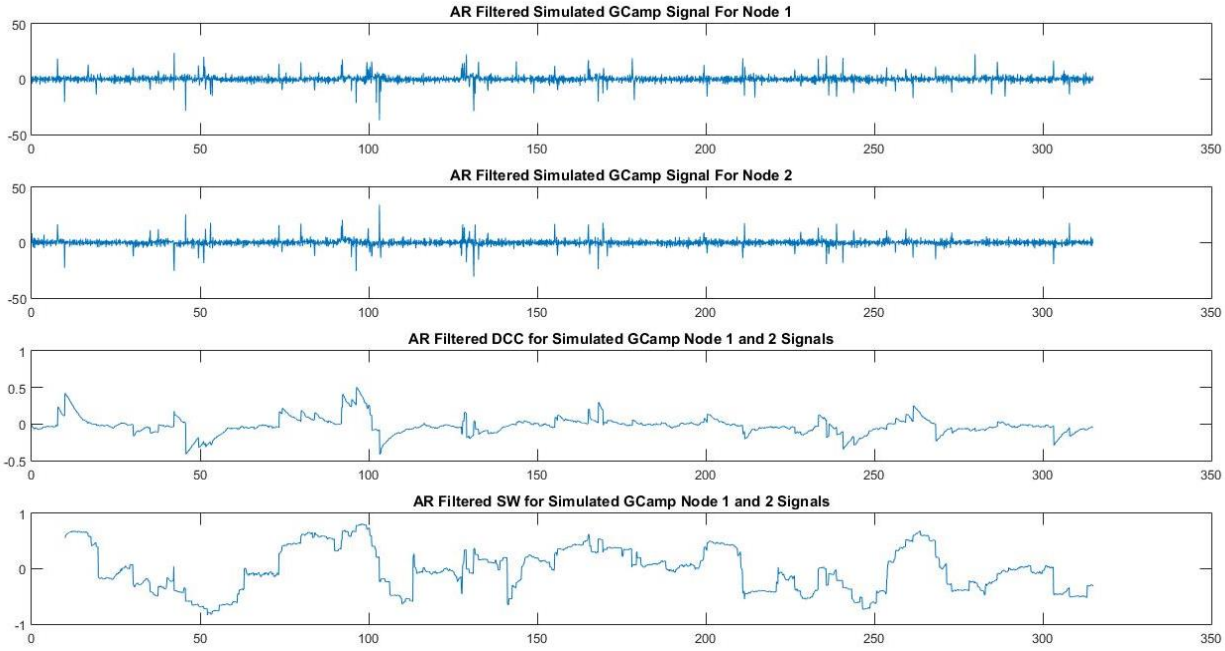

Figure 18. The plots here showcase how the AR filter represent the level-set of simulated GCAMP signals. The DCC has values that are realistic compared with the visualization of the nodes. There appears to be significant correspondence between DCC and SW as well The figure above shows binned (by factor 10) time points on the x-axis from 0 to 300 for the 5 minute movie sampled at 10 Hz. The y-axes show the values of amplitudes of the respective signals for the top two figures and the values of correlation coefficient, ranging between -1 to 1, for the bottom two figures.

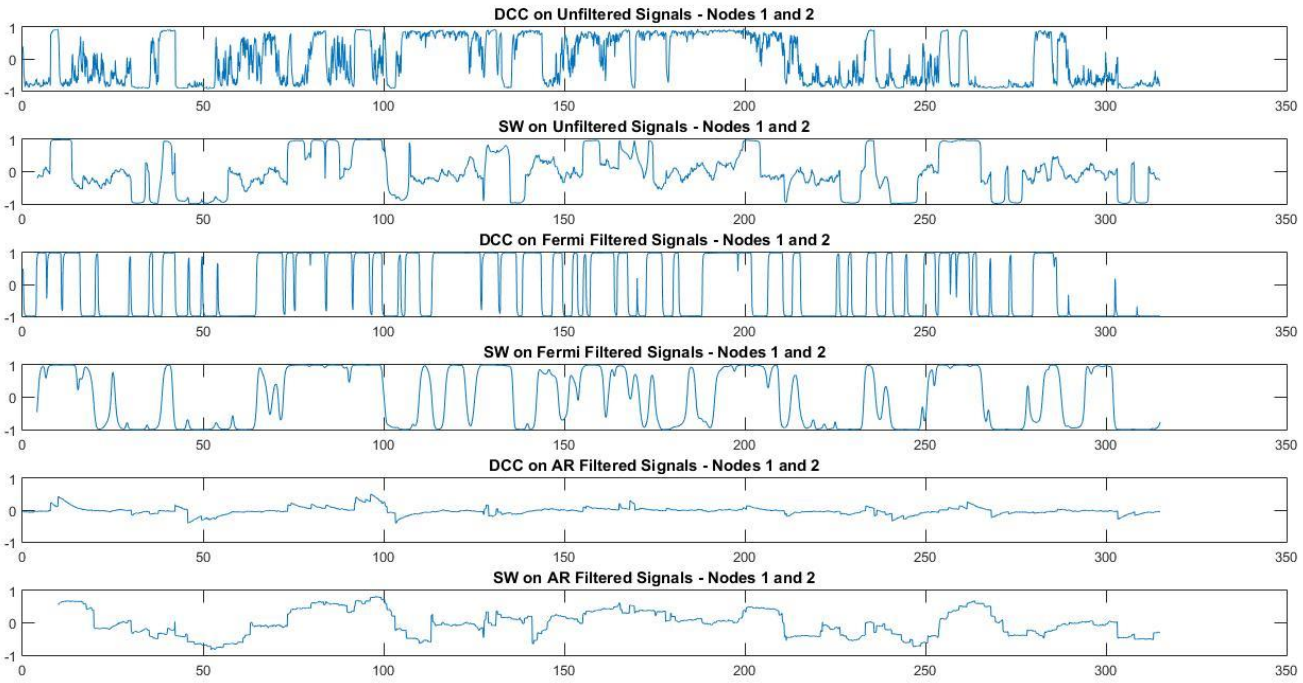

Figure 19. The plots here show how the DCC and SW vary with unfiltered, fermi filtered and AR filtered settings.The figure above shows binned (by factor 10) time points on the x-axis from 0 to 300 for the 5 minute movie sampled at 10 Hz. The y-axes show the values of amplitudes of the respective signals for the top two figures and the values of correlation coefficient, ranging between -1 to 1, for the bottom two figures.

3.6 SUMMARIZING METHODS APPLIED

Transgenic mice expressing GCaMP3, a fluorescent calcium indicator that reports changes in intracellular calcium concentration that accompany spiking activity [9], were used to simultaneously image ongoing changes in neuronal activity (GCAMP) as well as hemodynamic measurements of blood oxygenation (OIS-BOLD, analogous to fMRI) from the same animals (n=6). Bi-hemispheric GCAMP and OIS-BOLD images were acquired at 10 Hz from the exposed superior surface of the mouse brain under light ketamine anesthesia (30 mg/kg/hr) for 5 to 20 min periods. Pre-processing consisted of temporal band-pass filtering (0.02-0.20Hz). Then, k-means clustering was used on the GCAMP data to obtain 6 regions-of-interest (Figure 10) [6,7]. GCAMP and OIS-BOLD ROI time series were extracted for each mouse. We first examined the SW lengths for which the GCAMP and OIS-BOLD connectivity matrices were significantly correlated ($r>0.47$ corresponds to $p<0.05$). Over non-overlapping windows, the average SW correlation and fraction of significant windows are reported. We then examined the temporal sampling resolution for which comparisons between the GCAMP DCC and OIS-BOLD DCC connectivity matrices were significantly correlated.

3.7 RESULTS

For adjudging the dynamic characteristics of the neuronal and the hemodynamic fluctuations, specifically using non-stationarity based volatility methods, we found that auto-regressive (AR) filters worked better than previously used fermi filters. We carried out multiple

simulations on simulated GCaMP data with white noise and 1/f components and applied various volatility algorithms on it. The results obtained with AR filtered data matched the ground truth, however, those with fermi filtered data did not. This step is novel within our research practices. To focus on the neural/hemodynamic activities on the cortical surface, the blood vessels were excluded from further analysis. For this, large pial vessels were excluded by outlining masks for the visible cortical surfaces in both hemispheres. GCAMP (neuronal) and OIS-BOLD (hemodynamic) time series were used to calculate SW and DCC connectivity matrices (Figure 21). For each non-overlapping SW window, the inter-node connectivity of the GCAMP data was compared to that of the OIS-BOLD data and tested for significance using a correlation analysis. The average correlation shows significant relationships for window lengths over 20 sec, while the average fraction of significantly correlated windows was >80% for windows >40 sec (Figure 20). A similar analysis of the GCAMP and OIS-BOLD DCC connectivity shows that average significant relationships were observed for temporal resolution >1.4 sec, and >80% of the comparisons were significant for temporal resolution >2.2 sec. Adjusting for temporal lags between the GCAMP and OIS-BOLD time series did not alter these results.

3.8 CONCLUSIONS

The hemodynamic signals measured in this study were able to capture dynamic changes in neuronal connectivity over time scales of typical fMRI studies (>1-2 sec) using the DCC

algorithm. For SW methods, we observed significant agreement between hemodynamic and neuronal connectivity measurements for window lengths >20 sec. This means that DCC and SW have correspondences over 20 seconds, and that indicates that DCC's accuracy over 1-2 seconds can get us conditional correlation values at better temporal resolution.

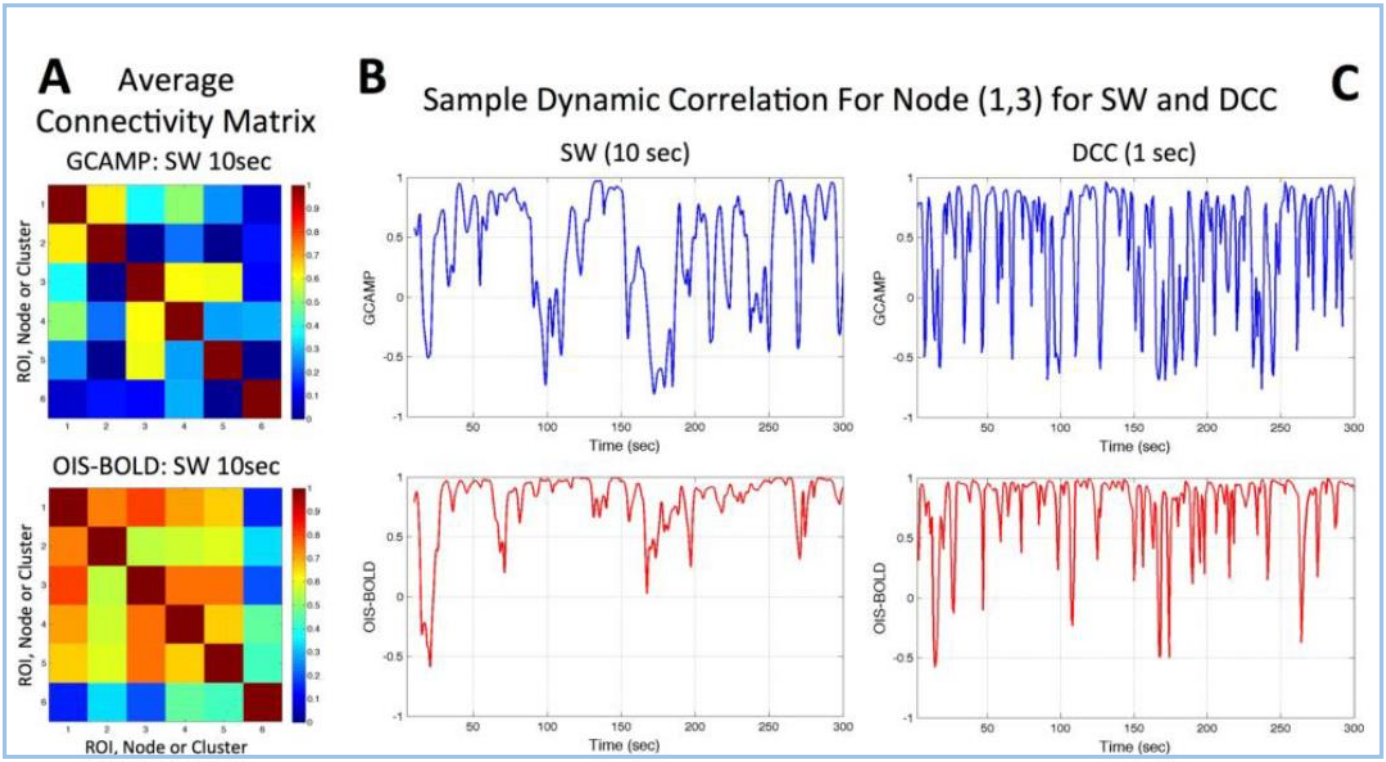

Figure 20. Results I: (A) Average correlation (connectivity) matrix calculated using SW (10-sec window length) from one subject for the GCAMP (top) and OIS-BOLD data (bottom). (B) Sample changes in correlation over time between nodes (ROIs) 1,3 calculated using SW (10-sec window length) in the same subject (top-GCAMP, bottom OIS-BOLD). (C) Sample changes in correlation between the same nodes (ROIs) (1,3) in the same subject calculated using DCC (1-sec data temporal resolution; top GCAMP, bottom OIS-BOLD).

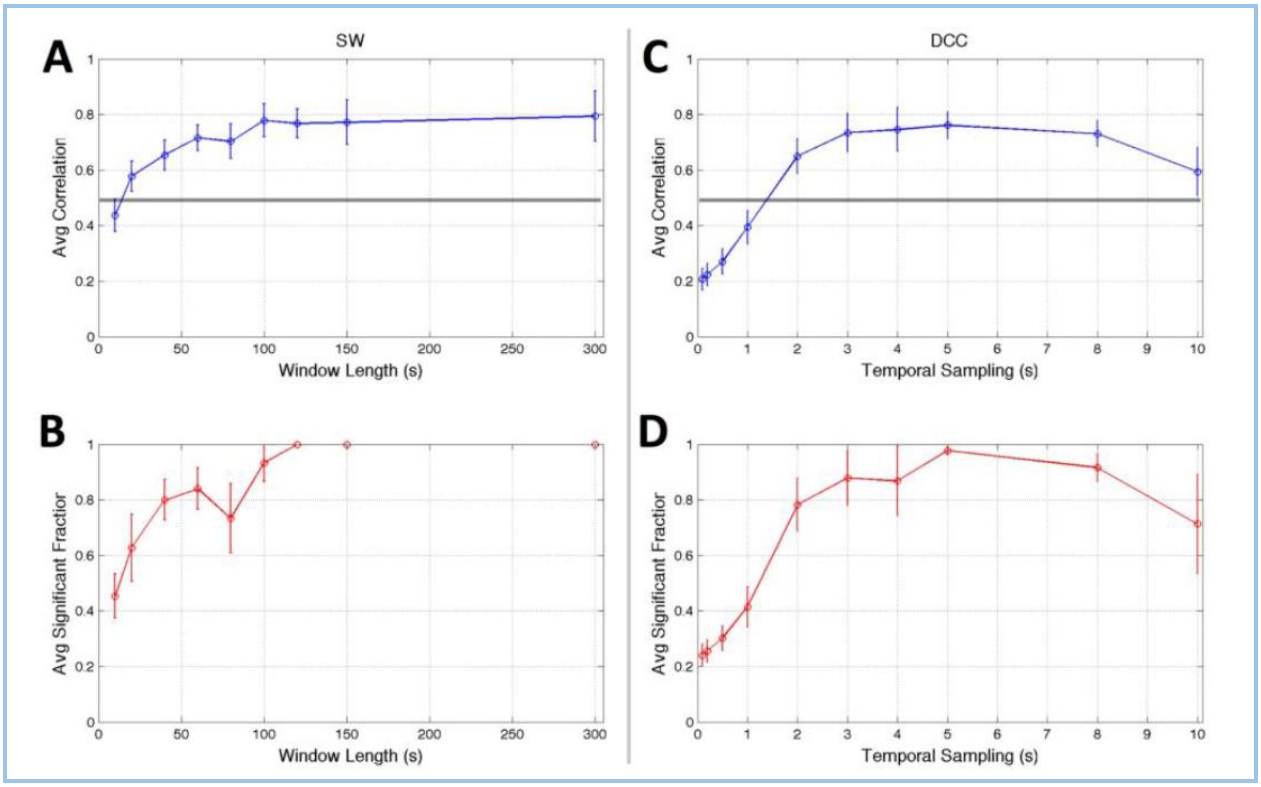

Figure 21. Results II: (A) Average correlation vs. SW window length across animals for the relationship between the inter-nodal GCAMP and OIS-BOLD connectivity over non-overlapping windows. (B) Average fraction of significant relationships in inter-nodal GCAMP and OIS-BOLD connectivity windows vs. SW window length. (C) Average correlation of the relationship between the inter-nodal GCAMP and OIS-BOLD connectivity calculated using DCC as a function of the data temporal resolution. (D) Average fraction of significant relationships between the GCAMP and OIS-BOLD connectivity vs. data temporal resolution. Error bars denote the standard error. Horizontal bar in A and C denotes significant threshold for individual tests ($p<0.05$).

BIBLIOGRAPHY

[1] Shmuel A. (2008), "Neuronal correlates of spontaneous fluctuations in fMRI signals in monkey visual cortex: implications for functional connectivity at rest", Human Brain Mapping 29:571.

[2] Mohajerani M.H. (2009), "Mirrored bilateral slow-wave cortical activity within local circuits revealed by fast bihemispheric voltagesensitive dye imaging in anesthetized and awake mice", Journal of Neuroscience 30:3745.

[3] Liu X. (2011), "Neural origin of spontaneous hemodynamic fluctuations in rats under burst-suppression anesthesia condition", Cerebral Cortex 21:374.

[4] Lu H. (2007), "Synchronized delta oscillations correlate with the resting-state functional MRI signal", PNAS 104:18265.

[5] Pan W.J. (2011), "Broadband local field potentials correlate with spontaneous fluctuations in functional magnetic resonance imaging signals in the rat somatosensory cortex under isoflurane anesthesia", Brain Connectivity 1:119.

[6] White B.R. (2011), "Imaging of functional connectivity in the mouse brain", PLOS one 6:e16322.

[7] Vazquez A.L. (2014), "Neuronal and physiological correlation to hemodynamic resting-state fluctuations in health and disease", Brain Connectivity 4:727.

[8] Lindquist MA (2014), “Evaluating dynamic bivariate correlations in resting-state fMRI: a comparison study and a new approach”, Neuroimage 101:531.

[9] Chen Q (2012), "Imaging neural activity using Thy1-GCaMP transgenic mice", Neuron 76:297.

[10] MacQueen, J. B. (1967). Some Methods for classification and Analysis of Multivariate Observations. Proceedings of 5th Berkeley Symposium on Mathematical Statistics and Probability. University of California Press. pp. 281–297. MR 0214227. Zbl 0214.46201. Retrieved 2009-04-07.

[11] Hutchison, R.M., Womelsdorf, T., Allen, E.A., Bandettini, P.A., Calhoun, V.D., Corbetta, M., Penna, S.D., Duyn, J., Glover, G., Gonzalez-Castillo, J., et al., 2013. Dynamic functional connectivity: promises, issues, and interpretations. NeuroImage 80, 360–378.

[12] Tsay, R.S., 2006. Multivariate volatility models. Lect. Notes Monogr. Ser. 210–222.

[13] Bauwens, L., Laurent, S., Rombouts, J.V., 2006.Multivariate Garchmodels: a survey. J. Appl. Econ. 21 (1), 79–109.

[14] Handwerker, D.A., Roopchansingh, V., Gonzalez-Castillo, J., Bandettini, P.A., 2012. Periodic changes in fMRI connectivity. Neuroimage 63, 1712–1719.

[15] Engle, R., 2002. Dynamic conditional correlation: a simple class of multivariate generalized autoregressive conditional heteroskedasticity models. J. Bus. Econ. Stat. 20 (3), 339–350.

[16] Bollerslev, T., 1986. Generalized autoregressive conditional heteroskedasticity. J. Econ. 31 (3), 307–327.

[17] Lebo, M.J., Box-Steffensmeier, J.M., 2008. Dynamic conditional correlations in political science. Am. J. Polit. Sci. 52 (3), 688–704.

[18] Allen, E.A., Damaraju, E., Plis, S.M., Erhardt, E.B., Eichele, T., Calhoun, V.D., 2012. Tracking whole-brain connectivity dynamics in the resting state. Cereb. Cortex. http://dx.doi.org/10.1093/cercor/bhs352.

[19] Sheppard, K., 2012. Forecasting high dimensional covariance matrices. Handbook of Volatility Models and Their Applications, pp. 103–125.

[20] Matteo Carndini et. el., 2015 Imaging the Awake Visual Cortex with a Genetically Encoded Voltage Indicator. Journal of neuroscience

[21] Hillman EM. Optical brain imaging in vivo: techniques and applications from animal to man. J Biomed Opt. 2007;12 doi: 10.1117/1.2789693. 051402.

[22] Pisauro MA, Dhruv NT, Carandini M, Benucci A. Fast hemodynamic responses in the visual cortex of the awake mouse. J Neurosci. 2013;33:18343–18351. doi: 10.1523/JNEUROSCI.2130-13.2013.

[23] Nagpaul, WinDAMS and IDAMS software, New Delhi, India

[24] Leon-Garcia Alberto, Probability and Random Processes for Electrical Engineering, Second Edition, 1994, University of Toronto